




Review Article

Steam Condensation Heat Transfer in the Presence of Noncondensable Gases (NCGs) in Nuclear Power Plants (NPPs): A Comprehensive Review of Fundamentals, Current Status, and Prospects for Future Research

Samah A. Albdour ^{1,2}, Yacine Addad ^{1,2}, Nourah Alyammahi,³ and Imran Afgan ^{1,2,4}

¹Department of Mechanical and Nuclear Engineering, Khalifa University, P.O. Box 127788, Abu Dhabi, UAE

²Emirates Nuclear Technology Center (ENTC), Khalifa University of Science and Technology, P.O. Box 127788, Abu Dhabi, UAE

³Federal Authority for Nuclear Regulation (FANR), P.O. Box: 112021, Abu Dhabi, UAE

⁴Department of Fluids and Environment, School of Engineering, University of Manchester, Manchester M13 9PL, UK

Correspondence should be addressed to Samah A. Albdour; 100058231@ku.ac.ae

Received 8 November 2023; Revised 5 March 2024; Accepted 25 March 2024; Published 25 April 2024

Academic Editor: Amin Shokrollahi

Copyright © 2024 Samah A. Albdour et al. This is an open access article distributed under the Creative Commons Attribution License, which permits unrestricted use, distribution, and reproduction in any medium, provided the original work is properly cited.

Efficient steam condensation is crucial for safe nuclear power plant (NPP) operations, preventing pressure buildup, overheating, and the release of radioactive materials. However, the presence of noncondensable gases (NCGs), such as air, nitrogen, hydrogen, or helium, can hinder the condensation process by creating a thermal resistance layer that impedes steam diffusion and condensation on the system's surface. Maximizing the efficiency of steam condensation requires a thorough grasp of the fundamental processes, theories, advancements, and technical hurdles. Therefore, this work thoroughly addresses these needs, with a particular emphasis on addressing the challenges posed by NCGs by dividing the work into four thematic areas. The first theme relates to a comprehensive examination of pure steam condensation phenomena, which includes an exploration of familiar condensation scenarios and various film condensation types. The second theme examines condensation in the presence of NCGs, their mixture properties, and related theories and modelling of heat and mass transfer. The third theme investigates condensation in NPP by exploring passive cooling systems and condensation phenomena under both natural and forced convection conditions during nuclear accidents, the origin of NCGs in NPP and their transportation aspects. This is followed by experimental work related to condensation scenarios and scale. Finally, the last theme looks upon the recent advancements in computational fluid dynamics (CFD) modelling of wall condensation, system analysis codes coupling with CFD, and the implementation of machine learning (ML) for predicting the condensation HTC. By bridging the gap between fundamental knowledge and practical applications, the four thematic areas presented in this work are aimed at providing a comprehensive foundation for researchers and experts in the field of steam condensation when NCGs are involved. The ultimate objective is to bolster the safety and efficacy of NPP operations by understanding the heat and mass transfer mechanisms while mitigating the risk of catastrophic events.

1. Introduction

Steam condensation is vital for ensuring the efficient functioning of the nuclear power plant's (NPP) cooling system under both routine operational conditions and unforeseen emergencies. Generally, the utilization of steam condensation is observed across multiple components of NPPs,

including condensers and steam generators for cooling purposes during normal operations as well as heat exchangers and emergency cooling systems during transient conditions. Advanced NPPs such as generation III and III+ incorporate passive containment cooling systems (PCCS) and spray systems [1, 2]. For instance, the PCCS units are designed to eliminate most of the decay heat during a loss-of-coolant

accident (LOCA) or main steam line break (MSLB) by promoting condensation of steam over specific heat transfer surfaces [3].

The significance of steam condensation is accompanied by a heightened probability of encountering noncondensable gases (NCGs) within the system. In 1929, Othmer [4] conducted a notable investigation that revealed how the inclusion of a minor quantity of NCG within pure vapor could significantly influence the condensation heat transfer coefficient (HTC), resulting in a notable reduction in the efficiency of heat transfer equipment. His findings demonstrated that as the volume fraction of air in the boiler increased from 0 to 0.5%, the surface heat transfer coefficient of the copper tube decreased by almost 50%. After Othmer's findings, various researchers [5–8] expeditiously corroborated his work by undertaking experimental investigations into condensation with a range of gases such as air, nitrogen, argon, or helium. The presence of these NCGs poses a detriment to the progression of condensation heat transfer, subsequently impeding the effectiveness of the condensation HTC. The presence of NCGs leads to the development of a diffusion layer near the condensate film, through which steam must permeate, resulting in an obstacle that reduces the effectiveness of the condensation heat transfer process [3]. (Further details of these phenomena are discussed in Sections 3 and 4.5.)

Over the years, many research articles have concentrated on investigating the condensation process in NPPs, examining factors like pressure changes, flow patterns, passive cooling systems, and heat transfer impacts. Table 1 provides a compilation of review papers presenting a summary of past articles that have examined steam condensation, along with their main areas of emphasis. To the knowledge of the authors, none of the previous reviews have provided a balanced assessment of the fundamentals, theories, experimental, and CFD studies, as well as the untapped potential of recent advancements in the research on steam condensation heat transfer when NCGs are present. In this regard, a comprehensive review of the existing literature is crucial, as it can provide valuable insights into the current state of knowledge and highlight areas for future research.

The primary objective of this review paper is to enhance the existing body of knowledge on condensation in NPPs in the presence of NCGs by summarizing and analyzing the findings of earlier research. The paper's novelty lies in its extensive analysis of the existing literature, with a particular emphasis on identifying knowledge gaps and research needs in the field. Overall, this review paper serves as a valuable resource for engineers and researchers working in the nuclear power industry, enabling them to gain a deeper insight into the complexities of condensation and its critical role in ensuring the safe and efficient operation of these facilities.

The present review is organised into six primary sections. The first section offers an introduction to the review paper, presenting its purpose and outlining the structure of the paper. Section 2 provides the basics of pure steam condensation phenomena, including the types and categorization of condensation. The third section delves into a

detailed description of the theoretical background of condensation in the presence of NCGs, including modelling approaches for heat and mass transfer with NCGs, effective diffusion coefficients, and mixture properties. The fourth section is exclusively devoted to the exploration of steam condensation heat transfer studies within NPPs. It commences with an introduction to passive cooling mechanisms and extends to cover the origins of NCGs and the dynamics of their transportation. This section also includes information on experimental and CFD studies, as well as containment thermal-hydraulic codes. Section 5 delves into the latest breakthroughs in steam condensation heat transfer investigations. Incorporated in this context is wall condensation for the CFD application, the utilization of a combined approach involving CFD and system analysis codes to enable multiscale simulation of wall film condensation within the heat structure, and advancements achieved in steam condensation heat transfer grounded on machine learning (ML) models. Finally, the sixth and last section provides conclusions and recommendations, serving as a guide for future research directions.

2. An Overview of Pure Steam Condensation Phenomena

Condensation takes place when the temperature of steam falls below its saturation point, which often happens in industrial equipment when the steam encounters a cool surface. As a result, the steam releases its latent energy, transfers heat to the surface, and undergoes condensation, resulting in the formation of condensate. Condensation can take place through various mechanisms; it can be homogeneous or heterogeneous. Homogeneous condensation refers to the condensation process taking place within the vapor phase itself, resulting in the formation of a fog-like cloud of condensate droplets. During the early phases of steam turbine operation, the emergence of condensate droplets poses the risk of causing blade erosion problems [18].

Heterogeneous condensation can occur in two ways, depending on the surface's condition, namely, dropwise condensation and film condensation. Dropwise condensation is a phenomenon characterized by the creation of discrete droplets on the surface responsible for heat transfer. This is primarily due to the surface's limited wetting ability, preventing the formation of a continuous liquid film. The behaviour of these droplets is influenced by their location and orientation relative to gravity, and once they reach a critical mass, they may detach from the surface. On vertical surfaces, droplets near the upper region rapidly descend once they achieve this critical mass, signifying the point at which gravity overcomes surface tension forces. Compared to film condensation, dropwise condensation typically results in significantly higher HTC, which has prompted extensive research efforts aimed at improving dropwise condensation [19].

In contrast, film condensation is a common phenomenon in industrial settings, occurring when a surface's temperature drops below the saturation temperature of steam, leading to the condensation of steam into a liquid film that

TABLE 1: A number of selected review papers on condensation phenomena.

Ref	Focus of study
[9]	Discusses the examination of steam condensation and hydrogen combustion in NPPs, with a focus on experimental investigations of both separate effects and large-scale experiments.
[10]	Provides a comprehensive examination of in-tube condensation, considering different tube positions (horizontal, vertical, and inclined) and enhancements like fins and inserts. While it offers valuable insights into condensation heat transfer, it solely focuses on the impact of these enhancements on the flow pattern of condensation, pressure drop, and void fraction and does not consider the potential effects of NCGs on the efficiency and safety of NPPs, particularly in terms of reactor containment physics.
[3]	Investigates the specific physical processes that occur during the condensation phenomenon and evaluates how they have been integrated into various models. It covers the progress made in experimental, mechanistic, and model-based research regarding condensation in the presence of NCGs. The article includes all research papers on this topic up to 2009.
[11]	Deals with a review analysis that utilizes flow mapping and compares its outcomes with CFD results. However, it is important to note that the impact of NCGs was not considered in this analysis.
[12]	Covers the advancements in the study of condensation with NCGs through experimental, mechanistic, and modelling research. The central emphasis primarily revolves around tangible representations of thermal transmission during film condensation accompanied by NCGs, while concurrently providing a succinct overview about dropwise condensation.
[13]	Reviews the attributes of heat transfer via external tube condensation, particularly within the framework of PCCS utilized in nuclear reactors.
[14]	Focuses on small modular reactor systems, with the reference reactor geometries being more closely aligned with in-tube wall condensation for downward steam flow.
[15]	Undertakes a meticulous and extensive examination of steam condensation amid NCGs during incidents at NPPs. The review underscores the in-depth scrutiny of the heat transfer procedure.
[16]	Provides an in-depth review of the literature on condensation heat transfer within containment structures involving NCGs. This encompasses summarizing and categorizing prior research, condensation models, and a detailed examination of the factors influencing the condensation process.
[17]	Addresses the behaviour of hydrogen within the containment during accident conditions and the corresponding advancements in research. This encompasses the distinctive characteristics of hydrogen behaviour, a compilation of key experiments and prediction methods related to hydrogen, and numerical simulations that consider various influencing factors and uncertainties.

covers the surface. Depending on the surface's geometry, this liquid film may flow under the influence of gravity and/or shear forces. As more steam condenses over time, the film's thickness increases in the direction of flow. At this stage, mass and heat transfer commence between the condensate and steam, whereby the film contributes to the additional resistance of heat transfer in comparison to an exposed solid surface. Despite the appearance of equilibrium between the two phases, there must be a decrease in temperature during condensation at or near the interface between the gas and liquid phases. Studies have shown that despite the condensate layer's resistance to heat transfer, the interface between the steam and liquid phases in pure steam is highly permeable to both heat and mass. Miller and Neogi [20] further suggested that the thickness of this interface can be as small as 1-2 molecular diameters, resulting in a significant increase in density and temperature gradients up to 108 K/m.

The force of gravity causes the downward movement of the liquid film in film condensation on a vertical flat plate, as shown in Figure 1. This downward flow may give rise to turbulence or cause the formation of a corrugated structure. When dealing with film condensation, it is crucial to differentiate between laminar and turbulent flow regimes. It is crucial to differentiate between laminar and turbulent flow regimes when solving the problem, as the approach heavily depends on the prevailing flow conditions. Condensed, free-falling films exhibit laminar, wavy-laminar, and turbulent flow regimes with various heat transfer properties,

depending on the Reynolds number (Re_{film}) of the film. The transition from laminar to turbulent flow occurs within a range of Reynolds numbers. Instead, there is a range of Reynolds numbers that cause the change. Therefore, it is more accurate to refer to a lower Reynolds number limit below which the flow remains laminar and a higher Reynolds number limit above which the flow is always turbulent.

Another well-known condensation case is in-tube reflux condensation, where the steam condenses into a liquid and flows in the opposite direction of the liquid condensate. Figure 2 illustrates the process of reflux condensation. In contrast to condensation occurring on a vertical flat plate, reflux condensation is characterized by the upward velocity of the steam, which creates a shear force that opposes the drainage of the condensate film. Strong steam shear prevents condensate drainage, causing it to be carried upwards by the steam, a phenomenon known as "flooding." Additionally, the tube flow is internal, which limits the available space and makes it prone to intense pressure oscillations in the event of flooding. These pressure fluctuations would lead to an unacceptably unstable performance of the devices that hold this structure for condensation [21].

Generally, when addressing film condensation in both scenarios, there are various thermal barriers to account for, but the most notable one is the resistance associated with the layer of condensed liquid on the surface. This resistance is considerably more substantial than the others. When the liquid film flows in a laminar manner, heat transfer

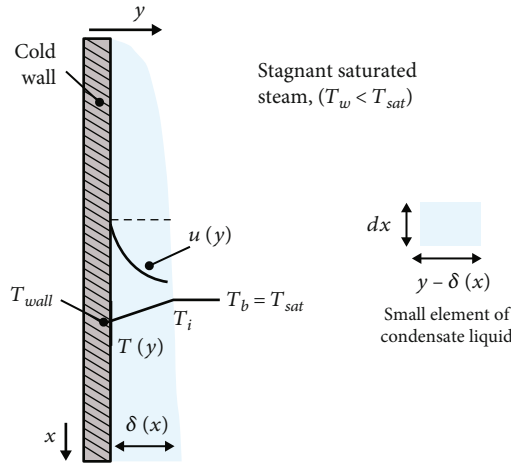


FIGURE 1: Condensation of a thin film on a flat, vertical plate.

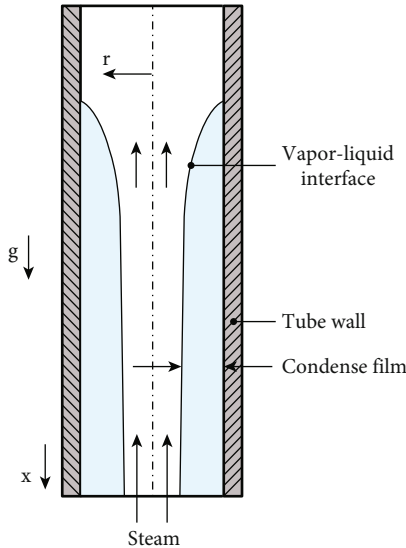


FIGURE 2: In-tube reflux condensation.

predominantly happens through conduction. Therefore, a thinner condensate film provides less resistance to heat transfer and consequently yields a higher heat transfer coefficient when compared to a thicker film. Moreover, condensation can take place on a vertical surface in either stationary or moving conditions. The force of gravity primarily shapes the liquid film in stationary situations, while the tangential forces resulting from the steam's velocity additionally influence it in dynamic scenarios. Factors impacting the condensation HTC encompass the speed of the steam, the thickness of the film, the turbulence in its motion, the existence of surface waves, the effects of drag and droplet deposition, instances of condensate splashing, and the degree of subcooling within the liquid. Following are the types of film condensation [22].

2.1. Gravity-Controlled Condensation. Nusselt was the pioneer in studying the laminar film condensation phenomenon and developed a straightforward yet efficient model

that remains in use to date to estimate the thickness of the film and the condensation rate. His research was centered on the case of pure steam condensing onto a vertical, flat surface. To simplify the calculations, Nusselt made several assumptions, some of which were explicitly stated while others were implied, as documented in [23–25].

- (i) The cooled surface is isothermal
- (ii) Dry saturated steam, balance vapor quality -1
- (iii) Condensate subcooling is not considered
- (iv) The thermophysical properties of the liquid are considered constant
- (v) The flow of the condensate film is laminar, and the surface of the film is smooth
- (vi) The vapor is stationary relative to the surface of the film
- (vii) Convective momentum transfer is not considered
- (viii) Convective energy transfer is not considered

Now, consider a vertical plate with dimensions “ L ” and “ w .” This plate is held at a steady surface temperature labelled as “ T_w .” This surface encounters a steam medium, with the temperature of the steam equating to the saturation temperature, identified as “ T_{sat} .” When this saturated steam contacts the cold surface, it will transform into liquid condensate on the plate. The temperature of the plate is lower than the saturation temperature ($T_w < T_{sat}$). If film condensation occurs, a continuous layer of condensate liquid will form on the surface of the vertical plate. Gravity and viscosity cause the condensate liquid film to flow downward, reaching the state shown in Figure 1.

The condensation process initiates at the top of the plate, where Figure 1 shows the origin set. In this setup, we can consider the positive x -direction to be pointing downward. As we move along the length of the plate, denoted by “ x ,” both the mass flow rate and thickness of the condensate film increase. Since the film of condensate presents a barrier to heat transfer, it must transport the heat from the steam to the plate. The speed of heat transfer will be slower when the thermal resistance of the film is higher [23]. The calculation of the heat transfer coefficient h_{nu} is conducted as follows.

$$h_{nu} = 1.47 \left[\frac{k_L^3 \rho_L (\rho_L - \rho_v) g}{\mu_L^2 Re_{film}} \right]^{1/3}, \quad (1)$$

where, k , ρ , and μ represent the thermal conductivity, density, and viscosity of the condensate liquid, respectively, and Re_{film} is the film Reynolds number, and it is expressed as $4\dot{m}_0/\mu\pi r$, where \dot{m}_0 represents the mass flow rate, μ is the dynamic viscosity, and r is the radius of the tube.

Therefore, we can express the Nusselt number (Nu_{film}) for the laminar film as follows:

$$Nu_{\text{film}} = 1.47 Re_{\text{film}}^{-1/3}. \quad (2)$$

The Nusselt theory, while providing a simplified explanation of condensation, necessitates the inclusion of several supplementary factors when comparing it to real-world experimental scenarios [22].

- (i) Subcooling occurs due to the temperature difference within the liquid film, resulting in the liquid at the wall being cooler than its saturation temperature, leading to a lower mean liquid temperature, T_1
- (ii) When considering vapor condensation over the liquid film, it is important to account for inertia as it is not a stationary process. Vapor needs to accelerate to match the velocity of the liquid film, introducing inertia effects
- (iii) When vapor is in a superheated state, it must undergo cooling from its initial bulk temperature to reach the saturation temperature at the interface. This cooling process introduces additional thermal resistance to the overall process
- (iv) A liquid film flowing downward generates interfacial waves, creating surface undulations. Certain experiments conducted by Van der Walt and Kroger [26] demonstrated that due to the presence of these waves, the measured heat fluxes were 5-10% higher than what the Nusselt theory had predicted
- (v) Practical scenarios commonly encounter turbulent film flow. The transition from laminar to turbulent flow within the film typically occurs within a Reynolds number ranging from 1600 to 1800

Considering the factors mentioned earlier, the calculation of the HTC in condensation processes governed by gravity (h_{grav}) is then determined as follows:

$$h_{\text{grav}} = 1.15 \left[0.0206 \left(\frac{h_{fg} \mu_l}{k(T_{\text{sat}} - T_w)} \right)^{0.5} + 0.79 \right] h_{nu}, \quad (3)$$

where h_{fg} is the latent heat of vaporization in J/kg.

Adding the multiplicative factor 1.15, as suggested by Baehr and Stephan [27], helps to explain why the average gravity-controlled HTC is bigger when film waves are present. Depew and Reisbig [28] suggested employing the term enclosed within square brackets to incorporate the inertia

effect. Finally, we compute the thermodynamic properties of the condensate at the mean temperature to consider liquid subcooling (T_l) as follows [18]:

$$T_l = 0.75T_{\text{wall}} + 0.25T_{\text{sat}}. \quad (4)$$

In the meantime, it is important to note that only the properties of the vapor are computed at the saturation temperature [29]. On the other hand, in turbulent regions, a typical correlation for condensation Nusselt number (Nu_{film}) is that of Labuntsov [30].

$$Nu_{\text{film}} = 0.023 Re_{\text{film}}^{0.25} Pr_{\text{film}}^{0.5}, \quad (5)$$

where Pr_l denotes the Prandtl number for the condensate liquid.

A comprehensive equation for determining the mean coefficient of falling film condensation on a flat plate, encompassing the combined influences of both wave and turbulence effects, is provided by Butterworth's formula [(29)].

$$Nu_{\text{film}} = \frac{Re_{\text{film}}}{8750 + 58Pr_{\text{film}}^{-0.5} (Re_{\text{film}}^{1.22} - 253)}. \quad (6)$$

2.2. Shear Controlled Condensation. At high vapor velocities, the dominant factor influencing the condensation HTC is the shear within the vapor phase. In fact, the influence of interfacial shear becomes significant when compared to the gravitational force acting on the liquid phase. The initial step in calculating the condensation HTC involves determining the flow regime of the liquid film, with laminar condensate flow being the most common situation. Exceeding a certain threshold, the vapor velocity neglects the gravitational impact on the two-phase process, leading to a condensation mode primarily governed by shear [22]. Subsequently, the calculation of $h_{\text{ss,laminar}}$ is performed as follows:

$$h_{\text{ss,laminar}} = \sqrt{\frac{k_l^2 \tau_w \rho_l}{2\Gamma_l \mu_l}}, \quad (7)$$

where Γ_l is the mass flow per unit periphery and τ_w is the shear stress at the wall.

In the case of turbulent flow, the calculation of condensation HTC can be done in the following manner [22]:

$$h_{\text{ss,turbulent}} = \frac{c_{p,l} (\rho_l \tau)^{1/2}}{T_{\delta}^+}, \quad (8)$$

where

$$T_{\delta}^+ = \delta^+ Pr_l \quad \text{for } \delta^+ \leq 5 = 5 \left[Pr_l + \ln \left\{ 1 + Pr_l \left(\frac{\delta^+}{5} - 1 \right) \right\} \right] \quad \text{for } 5 \leq \delta^+ < 30 = 5 \left[Pr_l + \ln \left\{ 1 + 5Pr_l \left(\frac{\delta^+}{5} - 1 \right) \right\} \right] + \frac{1}{2} \ln \left(\frac{\delta^+}{30} \right) \quad \text{for } \delta^+ > 30, \quad (9)$$

$$\delta^+ = 0.7071 Re_{\text{film}}^{0.5} \quad \text{for } Re_{\text{film}} \leq 50 = 0.6323 Re_{\text{film}}^{0.5286} \quad \text{for } 50 \leq Re_{\text{film}} \leq 1483 = 0.0504 Re_{\text{film}}^{0.875} \quad \text{for } Re_{\text{film}} > 1483.$$

2.3. Condensation under Combined Gravity and Shear Control. At intermediate vapor velocities, gravity starts to exert a notable influence on the shear stress dynamics. Consequently, under downflow conditions, τ_i is lower than τ_w . Butterworth's simplified approach from [31] calculates the HTC by considering both gravity and shear stress forces.

$$h = \sqrt{h_{\text{grav}}^2 + h_{\text{ss}}^2}, \quad (10)$$

where h_{grav} and h_{ss} are the coefficients calculated from equation (3) and equations (7) or (8).

It is worth highlighting that the Nusselt model and subsequent studies on pure steam condensation ([32–39]) did not take into account the presence of NCGs, even in small amounts, that can significantly reduce mass transfer rates. In fact, studies show that adding even small amounts of air can greatly lower the condensation HTC because it raises the concentration of NGC at the point where the liquid and steam mix. The condensate velocity accelerates towards the surface during the condensation process, which causes suction at the interface. As a result, air, for example, remains in the interface area, thereby increasing its concentration [40]. Consequently, this process leads to a reduction in the partial pressure of the steam, thereby causing a decrease in the steam saturation temperature. As a result, the thermal driving force for condensation diminishes, leading to a decline in the temperature difference between the wall and the condensation interface. This decrease in temperature ultimately leads to a decrease in the heat transfer rate. Additionally, the NCGs also act as a barrier between the steam and the wall, which necessitates the steam to diffuse through the gas layer to reach the condensate surface, further decreasing the heat transfer rate [3].

3. An Overview of Condensation in the Presence of NCGs

3.1. Basics of Steam Condensation in the Presence of NCGs. In engineering domains such as steam power plants, condensers are typically employed at pressures beneath atmospheric pressure, which can give rise to the ingress of air, exerting a significant impact on the condensation HTC, as evinced by practical tests and investigations ([41–43]). In general, if a smooth surface is cooler than the saturation temperature of water steam, a mixture of condensable and NCGs will course over it, creating nonequilibrium conditions. During steam condensation, there is a decline in its partial pressure, eliciting a suction effect that instigates the motion of steam from the bulk towards the cold wall. Along with the steam, the transport of NCGs towards the wall spawns two fluid layers, namely, the liquid boundary layer (LBL) and the gas boundary layer (GBL), as depicted in Figure 3. Inside the GBL, there is a relatively elevated partial pressure of NCGs when compared to the overall mixture. This discrepancy in partial pressure gives rise to a diffusion force that impels the NCGs towards the bulk region. Furthermore, the reduced partial pressure of steam at the interface between the liquid-vapor/gas phase and the

surrounding medium generates a force that propels steam through the GBL. This phenomenon leads to convective motion of the mixture and establishes a circulation flow within the system.

The convection of gases aids in the mixing of the bulk and the boundary layers, thereby improving condensation heat transfer. Despite this beneficial driving force, the condensation process typically confronts three thermal resistances linked in a sequence, as depicted in Figure 3. To overcome the thermal resistances, one must address the convective resistances in both the LBL and GBL, as well as the conductive resistance of the cold wall where condensation occurs. Stephan [44] and Carey [45] have delved into investigations into these impediments. The resistance across the GBL can be subdivided into two segments: one for condensation HTC and the other for convective HTC induced by the motion of NCGs. These two segments are linked in parallel, and the aggregate equivalent resistance ($1/h_g$) is computed by invoking the principles of heat and electrical transport analogy [45].

$$h_g = h_{\text{cond}} + h_{\text{conv}}. \quad (11)$$

The formula widely recognized for representing the HTC in natural convection condensation is expressed as follows [46]:

$$h = \frac{k\text{Nu}}{L} = 0.0295\text{Gr}_L^{2/5}\text{Pr}^{7/15}(1 + 0.494\text{Pr}^{2/3})^{-2/5}. \quad (12)$$

Thus, the overall thermal resistance can be expressed as

$$\frac{1}{h_{\text{tot}}} = \frac{1}{h_l} + \frac{1}{h_g}, \quad (13)$$

where $1/h_{\text{tot}}$ represents the total thermal resistance while $1/h_l$ and $1/h_g$ signify the resistance contributed by the LBL and GBL, respectively. It is important to note that the conductive resistance of the cold wall is typically excluded from the outcomes presented in the literature. Researchers commonly employ this approach to demonstrate that the resistances offered by the physical phenomena at play, namely, the LBL and GBL, are the only factors influencing heat transfer results. The determination of these resistances holds great significance in numerous engineering scenarios. They are crucial in the evaluation of the natural circulation pattern and the resulting composition of the local mixture in complex systems like reactor containments.

On the other hand, the buoyancy force causes significant interfacial resistance due to the overall density difference between the wall or interface and the bulk. The degree to which buoyancy forces affect the flow field and transport processes depends on the free stream velocity of the mixture, and their ratio, known as the Richardson number (Ri), can

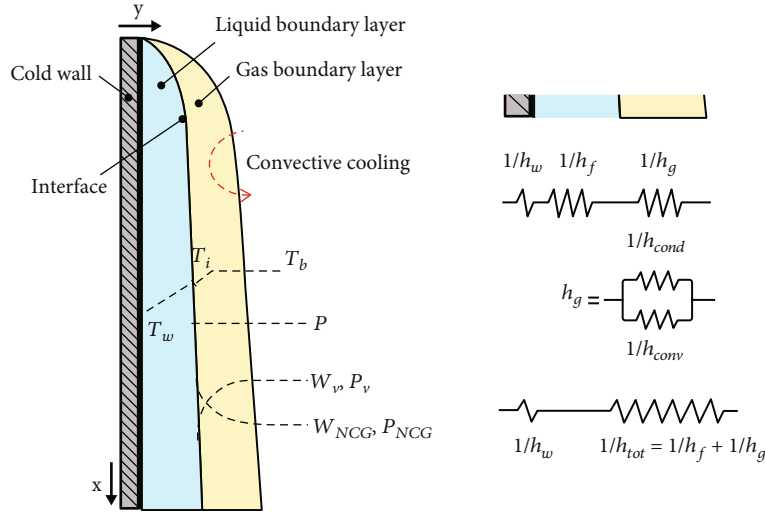


FIGURE 3: Profiles of concentration, pressure, and temperature in a condensed steam-air mixture.

be used to determine the dominant contribution of buoyancy and inertia forces [47].

$$Ri = \frac{Gr}{Re^2}, \quad (14)$$

where Gr represents the Grashof number.

In situations where buoyancy forces surpass inertia forces, or when $Ri \gg 1$, it is probable that natural convection regimes will emerge. Conversely, when inertia forces are dominant and $Ri \ll 1$, the convection regime becomes forced. Mixed convection regimes arise when buoyancy and inertia forces are of commensurate magnitude, i.e., when $Ri = 1$. Moreover, buoyancy forces impact transport properties in the region of mixed convection in two ways. When buoyancy and inertia forces coexist in the same direction, this is denoted as “buoyancy-aided” mixed convection [47].

$$(\rho_i - \rho_b) \vec{g} \cdot \vec{U} > 0. \quad (15)$$

On the other hand, when buoyancy forces and inertia forces act in opposite directions, it is referred to as “buoyancy-opposed” mixed convection [47].

$$(\rho_i - \rho_b) \vec{g} \cdot \vec{U} < 0, \quad (16)$$

where \vec{U} represents the mixture velocity. The readers are encouraged to see [47] for further details.

3.2. Theoretical Background of Condensation in the Presence of NCGs

3.2.1. Effective Diffusion Coefficient and Mixture Properties. The condensation of steam on a vertical surface is dependent on various factors, including the properties of the steam, the characteristics of the surface, and the specific conditions under which the condensation occurs. The effective diffusion coefficient and the mixture properties are two fundamental

properties that can be utilized to depict this process. The effective diffusion coefficient is an indicator of the rapidity with which the steam can traverse from the steam’s bulk to the surface, where condensation occurs. This coefficient accounts for the diffusion of the steam through the NCGs and takes into consideration the effects of the surface on the steam’s motion. One can compute the effective diffusion coefficient by employing a variety of models, depending on the specific conditions inherent to the system.

A multitude of models in the existing literature approximate the effective diffusion coefficient of steam in a convection with NCGs. Wilke and Lee’s method [48] is commonly used among these models and can be represented by the following equation:

$$D_{v,g} = \frac{1 - X_v}{\sum_{j,j \neq v} (X^j / D_v^j)}, \quad (17)$$

where X^j is defined as follows [9]:

$$X^j = \frac{P_{tot} - P_{sat,g}}{P_{tot}}. \quad (18)$$

Some researchers [49] utilize mass fractions in the assessment of the diffusion coefficient:

$$D_{v,g} = \frac{1 - W_v}{\sum_{j,j \neq v} (W^j / D_v^j)}. \quad (19)$$

Researchers in the literature employ different definitions of average temperature to determine the gas properties within the diffusion layer. Calculating the mass and mole fractions is based on the bulk conditions.

In addition, there are multiple equations utilized to calculate the binary diffusion coefficient, denoted as D_v^j . According to the kinetic theory of gases, binary diffusion coefficients in gases are inversely proportional to the pressure or density at low to moderate pressures, and they do

not depend on the mixture's composition. The following formula is an estimation of the binary diffusion coefficient.

$$D_v^j(P, T) = \frac{a}{P \times 10^{-5}} \left(\frac{T}{273.15} \right)^n. \quad (20)$$

Table 2 consists of a comprehensive list of coefficients (a) and (n) associated with each species. These coefficients are employed in equation (24) to facilitate calculations and estimations.

Another approach involves employing the Fuller correlation model, as described in [50], to estimate the binary diffusion coefficient between steam (v) and a species (j). This correlation model provides a reliable means of estimating the diffusion coefficient for such binary mixtures.

$$D_v^j(P, T) = \frac{0.0143T^{1.75}}{P(W_{v,j} \times 10^3)^{1/2} \left[(\Sigma_v)_v^{1/3} + (\Sigma_v)_j^{1/3} \right]^2}, \quad (21)$$

where Σ_v is the volumetric diffusion for different species and $W_{v,j}$ is defined as follows:

$$W_{v,j} = 2 \left(\frac{1}{W_v} + \frac{1}{W_j} \right)^{-1}. \quad (22)$$

Equation (21), which represents the Fuller model, can be expressed in the form of Equation (20), which is similar to the formula used to calculate the binary diffusion coefficient as mentioned earlier.

$$D_v^j = \frac{a'}{P \times 10^{-5}} \left(\frac{T}{273.15} \right)^{1.75}, \quad (23)$$

where a' values are available in Table 2.

It is noteworthy to highlight the significance of choosing an efficient model for the diffusion coefficient, as emphasized by Benteboula and Dabbene [51]. The impact of D_v^j modelling on heat and mass transfer is notably more substantial than the influence of heat and mass transfer correlation, especially when dealing with light gas.

On the other hand, the properties of the mixture refer to the combined qualities of the air and steam that surround the surface, such as viscosity, density, and thermal conductivity. These mixture properties are crucial in determining the rate of condensation, as they influence the exchange of mass and heat between the surface and the surrounding air. To accurately predict the rate of condensation on a surface, it is necessary to consider both the mixture properties and the effective diffusion coefficient. These models can incorporate relevant physical phenomena like fluid dynamics, heat transfer, and diffusion to achieve this. Ultimately, engineers can use these models to optimize the design of heat and mass transfer systems, such as condensers and evaporators. The properties are calculated using the relationships mentioned below [50].

$$\mu_m = \sum_{i=1}^n \frac{X_i \mu_i}{\sum_{j=1}^n X_j \phi_{ij}}, \quad (24)$$

$$k_m = \sum_{i=1}^n \frac{X_i k_i}{\sum_{j=1}^n X_j \psi_{ij}}, \quad (25)$$

$$c_{p,m} = \sum_{i=1}^m W_i c_{p,i}. \quad (26)$$

The calculation of the Wilke (ϕ_{ij}) and Mason-Saxena (ψ_{ij}) terms involves the use of a specific mathematical expression, as follows:

$$\begin{aligned} \phi_{ij} &= \frac{1}{\sqrt{8}} \left(\frac{M_j}{M_i} \right) \left(\frac{M_i}{M_i + M_j} \right)^{1/2} \left[\left(\frac{M_i}{M_j} \right)^{1/4} + \left(\frac{\mu_i}{\mu_j} \right)^{1/2} \right]^2, \\ \psi_{ij} &= \phi_{ij} \left[1 + \frac{2.41(M_j - M_i)(M_i - 0.142M_j)}{(M_j + M_i)^2} \right]^2. \end{aligned} \quad (27)$$

3.2.2. Modelling of Heat and Mass Transfer with NCGs. Researchers have developed various models to assess the adverse effects of NCGs that accumulate near the condensate layer. Semitheoretical and theoretical models broadly classify these models into two categories. Semitheoretical models encompass the degradation factor model and the heat and mass transfer analogy (HMTA) model with a wall function. These models are pragmatic and relatively straightforward to use, providing practical estimations of the impact of NCGs on condensation processes. The diffusion boundary layer (resolved boundary layer) model within the framework of heat and mass transfer diffusion (HMTD), on the other hand, uses mathematical physics equations to give a more complete picture of the condensation process when NCGs are present. These models go into more detail about the complicated nature of the phenomenon by using diffusion boundary layer ideas and looking at how different factors that affect condensation with NCGs interact with each other. Semitheoretical models are often favoured for their simplicity and practicality, while theoretical models provide a more detailed understanding by incorporating fundamental principles and equations to model condensation with NCGs [12].

(1) Semitheoretical Models.

(i) Degradation Factor-Based Model

The methodology of the degradation factor, originally presented by Vierow [52], laid the groundwork for the initial framework. This method uses the idea of a degradation factor (f), which is the ratio between the condensation HTC seen in the experiment and the HTC connected with pure steam condensation, as found by Nusselt analysis as depicted in equation (28). Subsequently, we link the degradation

TABLE 2: Coefficients for binary diffusivity estimation.

Equation no.	Gas	H ₂ O	N ₂	O ₂	He	H ₂
(20)	a	2.77×10^{-5}	2.27×10^{-5}	2.40×10^{-5}	7.30×10^{-5}	7.80×10^{-5}
	n	0.0	1.75	1.71	1.75	1.75
	\sum_v	13.1	18.5	16.3	2.67	6.12
(23)	a'	2.78×10^{-5}	2.24×10^{-5}	2.28×10^{-5}	7.31×10^{-5}	7.86×10^{-5}

factor to the attributes of the gas mixture, which include the Reynolds number and the mass fraction of NCGs. Through the establishment of these correlations, the model bestows valuable insights into the influence exerted by NCGs on the condensation process.

$$h_{\text{cond}} = f(\text{Re}_g, w_a) h_{\text{Nu}}. \quad (28)$$

Terasaka and Makita [53] developed another degradation factor that is related to the mass fraction of NCGs. Their factor was fitted to various experimental and numerical databases ([54–56]) in the range of 0–1 mass fractions. Their correlation has been compared to the database of Vierow and Schrock [57], and the results are positive across the board. However, there is some scattered data that the correlation could not replicate. Nevertheless, the very various experimental setups utilized to fit the correlation provide the model with a broad range of applications. Meanwhile, Kuhn et al. [58] undertook a series of experiments concerning film condensation occurring within a vertical tube infused with a combination of air and helium. They were able to find a link between the degradation factor and the ratio of film thickness during condensation when NCGs were present compared to when pure steam was present. They established this correlation by considering the influential factors of the Reynolds number for film thickness and the mass fraction of NCGs.

Lee and Kim [59] embarked on a comprehensive investigation, encompassing both experimental and theoretical aspects, to expand upon existing knowledge in the field. Their study focused on elucidating the intricate mechanisms governing local heat transfer within the small-diameter vertical tube in the presence of NCGs. Through meticulous testing, they acquired valuable insights and proposed an innovative correlation that considers condensation and the degradation factor. This correlation serves as a tool to assess how the condensate flow rates and the mass fraction of NCGs impact the HTC.

To facilitate understanding, Table 3 presents a compilation of the previous correlations for degradation factors, accompanied by their respective parameters.

(ii) Heat and Mass Transfer Analogy- (HMTA-) Based Model

Colburn and Hougen first introduced the notion of similarity between the mechanisms of heat transfer and mass diffusion in their seminal work [60]. Shortly thereafter, in

the same year, Chilton and Colburn derived an equation that encapsulates this analogy [61]. By employing this equation, it is possible to compute the rate of mass diffusion by considering the relationship between the change in partial pressures and the average difference in partial pressures between the gas mixture and the surface. The ratio of the temperature differential to the average difference in temperatures establishes the rate of heat transfer. The HMTA technique appraises the condensation HTC by gauging the mass of condensate or diffused substance.

The computation of condensate mass transfer is typically performed using established mass flux equations found in the existing literature. These equations heavily rely on the formulation of Fick's law of diffusion, which is extensively elucidated in [62]. The two formulations for mass flux are the mass approach (\dot{m}_i'')_{mass}, as utilized in [63–65], and the molar approach (\dot{m}_i'')_{molar}, as employed by [62], as referenced in relation to [65, 66]. (Diverse formulations of the heat and mass transfer analogy are detailed in [66].)

Mass approach:

$$\left(\dot{m}_i''\right)_{\text{mass}} = \text{Sh}_{g,0} \frac{\rho_g D_g}{L} \ln \left(\frac{w_{\text{NCG},b}}{w_{n,i}} \right). \quad (29)$$

Molar approach:

$$\left(\dot{m}_i''\right)_{\text{molar}} = M_v \text{Sh}_{g,0} \frac{c_g D_g}{L} \ln \left(\frac{X_{\text{NCG},b}}{X_{\text{NCG},i}} \right). \quad (30)$$

In the context above, $\text{Sh}_{g,0}$ represents the Sherwood number pertaining to low mass transfer rates, and c_g represents molar concentration, in mole/m³. Applying the HMTA and assuming turbulent and naturally driven gas mixture flow, we can express the Sherwood number in a manner analogous to the McAdams correlation for free convective flows [67]:

$$\text{Sh}_{g,0} = 0.13(\text{GrSc})^{1/3}, \quad (31)$$

where Sc denotes the Schmidt number.

And for forced convection, it is presented as follows [46]:

$$\text{Sh}_{g,0,FC} = 0.037 \text{Re}^{-0.2} \text{Sc}^{-2/3}. \quad (32)$$

Both equations presume that diffusion into the surrounding bulk adequately counterbalances the convective

TABLE 3: Degradation factor correlations and their parameters.

Author (year)	Degradation factor correlations	Parameters				
Vierow (1990) [52]	$f(\text{Re}_g, w_a) = (1 + a \text{Re}_g^b)(1 - cw_a^d)$	w_a	a	b	c	d
		$w_a < 0.063$	2.88×10^{-5}	1.18	10	1
		$0.063 < w_a < 0.6$	2.88×10^{-5}	1.18	0.94	0.13
Terasaka and Makita (1997) [53]	$f(w_a) = [1 - 0.964w_a + 4.989w_a^2 - 4.135w_a^3] \cdot \left(\frac{1 - w_a}{1 + 15.48w_a}\right)$	$0 < W_a < 1$				
Kuhn et al. (1997) [58]	$f\left(\frac{\delta_{\text{exp}}}{\delta_{\text{Nu}}}, \text{Re}_l, w_a\right) = \frac{\delta_{\text{exp}}}{\delta_{\text{Nu}}}(1 + a \text{Re}_l)(1 - bw_a^c)$	w_a	a	b	c	
		$w_a < 0.1$	7.23×10^4	2.6	0.708	
		$w_a < 0.1$	7.23×10^4	1	0.202	
		$w_a < 0.01$	7.23×10^4	-35.8	1.074	
Lee and Kim (2008) [59]	$f(\tau_g, w_a) = \tau_g^{*0.3124}(1 - 0.964w_a^{0.402})$	$0.06 < \tau_g^* < 46.65$		$0.038 < w_a < 0.814$		

flow of NCGs at the interface. Additionally, Ambrosini et al. [66] demonstrated that for a substantial range of condensation-related conditions, the variations between the two values obtained from the two approaches are within a few percentage points. It is only in instances of significant differences in molar fractions between the bulk fluid and the interface that the disparity reaches values of 10% and beyond, reaching up to 22% in extreme cases.

(2) Theoretical Models.

(i) Heat and Mass Transfer Diffusion- (HMTD-) Based Model

The diffusion layer model is a more accurate representation of mass transfer than the HMTA model due to its consideration of temperature gradients and thermal resistances. The presence of NCGs affects steam condensation not only through temperature and pressure but also due to these aforementioned factors, as highlighted in previous studies [68, 69]. To address this limitation, the Clausius-Clapeyron equation has been employed to incorporate these factors into the models [69–72]. There are three ways that heat moves during condensation: sensible heat moves across the gas boundary layer, latent heat is exchanged at the interface, and heat moves through the condensate film. As a result, throughout the condensation process, steam encounters thermal resistances originating from convection, condensation, and conduction that it must overcome.

In their study, Peterson et al. [69] used a better version of the Clausius-Clapeyron equation, which shows how the partial pressure or density gradient changes as the saturation temperature changes. The researchers expressed the equation as follows:

$$\frac{\Delta P}{\Delta T} = \frac{h_{fg}}{T_{\text{avg}} v_{fg}}. \quad (33)$$

Within the Clausius-Clapeyron equation, the mean values of h_{fg} and v_{fg} were employed, with these values being determined using the average temperature as a reference. The approximation for the specific volume difference (v_{fg}) between steam and liquid is given by the following:

$$v_{fg} = \frac{RT_{\text{avg}}}{M_V X_{v,\text{avg}} P_t}, \quad (34)$$

where $X_{v,\text{avg}}$ is the steam log mean molar fraction and defined as follows:

$$X_{v,\text{avg}} = \frac{X_{v,b} - X_{v,i}}{\ln(X_{v,b}/X_{v,i})}. \quad (35)$$

Peterson et al. [69] referred to the inverse unit of thermal conductivity present in the last term of the aforementioned expression as the “effective condensation thermal conductivity” (k_{cond}), which was calculated as the inverse of this term. The integration process can be used to determine the condensation mass flux (\dot{m}_{cond}) that considers changes in the molecular weight and density of the mixture as it passes through the diffusion layer in accordance with the principle of mass conservation.

$$\int_b^i \dot{m}_{\text{cond}} dy = \int_b^i - \frac{\rho_{\text{mix}} D}{1 - W_v} dW_v. \quad (36)$$

The amount of heat that is given off when condensation happens is the same as the amount of heat that moves through the liquid film.

$$\frac{k_{cd}(T_b - T_i)}{\delta_{\text{mix}}} = h'_{fg} \dot{m}_{\text{cond}}, \quad (37)$$

where δ_{mix} is the diffusion boundary layer thickness, and k_{cd} is defined as follows:

$$k_{cd} = \frac{\varnothing_2 h'_{fg} D M_v^2 P}{\varnothing_1 R^2 T_{avg}^3}, \quad (38)$$

where

$$\begin{aligned} \varnothing_1 &= \frac{\ln(W_{v,b}/W_{v,i})}{\ln((1-W_{v,i})/(1-W_{v,b})) \cdot [(M_g W_{v,b} + (1-W_{v,b})M_v)/(M_g W_{v,i} + (1-W_{v,i})M_v)]}, \\ \varnothing_2 &= \frac{\bar{M}_m M_g}{(M_{m,b} M_{m,i})}, \end{aligned} \quad (39)$$

where M_v and M_g are the steam and NCG molecular weight, respectively; T_{avg} is the average temperature of the interface and bulk; M_m is the mixture molecular weight, $M_m = X_v M_v + (1-X_v)M_g$; \bar{M}_m is the average mass mixture molecular weight, $\bar{M}_m = 1/((\bar{W}_v/M_v) + (1-\bar{W}_v)/M_g)$; and \bar{W}_v is the log mean mass fraction, $\bar{W}_v = (W_{v,b} - W_{v,i})/\ln(W_{v,b}/W_{v,i})$.

By incorporating the effective condensation thermal conductivity, also known as condensation conductivity, we can calculate the total resistance to heat transfer by considering both the condensation HTC and the sensible/convective HTC in parallel, along with the liquid resistance in series.

$$h_{tot} = \frac{h_l(h_{conv} + h_{cond})}{h_l + h_{conv} + h_{cond}}. \quad (40)$$

Next, we computed the transfer of heat from the bulk to the cooled wall using Equation (45) in the following manner:

$$q_t = h_{tot}(T_b - T_w). \quad (41)$$

Herranz et al. [72] proposed an improved version of the model discussed earlier. This revised model removes the assumption of a constant v_{fg} value and instead estimates the volume of steam using ideal gas equations. The model by Peterson et al. [69], which analyzed a specific temperature range, made use of a mean value for v_{fg} :

$$v_{fg} = v_g - v_i = \frac{R_g T}{P_g} - v_i. \quad (42)$$

In Herranz's analysis, Equation (42) was employed instead of Equation (34), and as a result, other parameters were adjusted accordingly. Ultimately, the condensation HTC was computed as follows:

$$h_{cond} = \left(\frac{Sh}{L}\right) k_{cd}. \quad (43)$$

Equation (40) incorporates both convective and liquid HTC, which are determined using correlations that were specifically developed for severe nuclear accidents. These correlations were formulated to account for the turbulent natural convection flow that typically arises from a sudden

initial blowdown event. For determining the convective HTC in these hypothetical scenarios, Herranz et al. [72] utilized the McAdams correlation, which is well suited for turbulent conditions.

$$h_{conv} = 0.13 \frac{k_g}{L} Gr^{1/3} Pr^{1/3}. \quad (44)$$

In this context, the Grashof number was defined as follows:

$$Gr = \frac{\rho_{g,b}(\rho_{g,i} - \rho_{g,b})gL^3}{\mu^2}. \quad (45)$$

The Grashof number definition, which concentrates on the density difference across the interface, was found to be advantageous in accurately estimating the condensation HTC. This method made it easier to figure out the sudden change in densities across the interface. It also made it easier to figure out how the hydrogen gas would separate in the upper compartment by giving a more accurate estimate of the buoyancy force. The modified Nusselt equation was used to calculate the liquid HTC (h_l), as shown below [73]:

$$h_l = \left[\frac{\rho_l(\rho_l - \rho_v)gh'_{fg}k_l^3}{4\mu_l x(T_i - T_w)} \right]^{1/4} \Psi_{fw}. \quad (46)$$

The variable Ψ_{fw} considers the effect of waviness on the condensate film, which enhances heat transfer. Then, the total HTC can be determined by using Equation (46).

On the other hand, Liao and Vierow [65] introduced a solid correlation rooted in the diffusion layer model expressed by the following:

$$h = \frac{h_{fg} \rho_{mix} D}{\delta_g (T_b - T_i)} \ln \left(\frac{1 - w_{v,i}}{1 - w_{v,b}} \right), \quad (47)$$

where δ_g is the thickness of diffusion layer (m).

In summary, the HMTA method offers a broader application scope, allowing for the study of heat and mass transfer in fluids regardless of their position within the fluid [47]. In contrast, the HMTD method is a more specialized approach that specifically focuses on heat and mass transfer at boundaries, making assumptions about the flow, concentration, or temperature gradient near the boundary. The HMTD approach is particularly effective in predicting heat and mass transfer coefficients at interfaces and considers the influence of NCGs on the condensation process through mass transfer effects. It can be applied to various condensation scenarios involving different fluids, geometries, and pressure conditions [74]. However, the HMTD model does have some limitations. One challenge is the scarcity of detailed experimental data regarding the behaviour and properties of NCGs near the interface. Furthermore, a refined mesh becomes imperative in the vicinity of the boundary region owing to the steep gradient exhibited by

the species mass fraction [75]. This necessity stems from the computational demands imposed by the HMTD model, particularly when confronted with intricate geometries and multiphase flows. Despite these limitations, the HMTD model demonstrates a higher level of consistency with empirical data compared to other models based on experimental correlations or the HMTA approach, regardless of system geometry, flow dynamics, or the nature and composition of NCGs. It is important to note, however, that for NPPs licensing purposes, HMTA and its associated correlations are more commonly used and preferred over HMTD. Furthermore, most thermal-hydraulic codes utilized for containment modelling heavily rely on HMTA and its derived correlations (more details are presented in Section 4.5).

4. Condensation in NPPs and Relevant Studies

4.1. Passive Cooling System. In a NPP, the process of condensation plays a crucial role in extracting heat from the reactor core and effectively regulating the temperature and pressure of the coolant. However, insufficient condensation of steam can result in increased pressure and temperature within the reactor, surpassing established safety limits. This escalation increases the risk of a nuclear accident, potentially damaging the containment wall due to the decay heat generated in the core. Illustrated in Figure 4 are various types of condensation phenomena observed in NPPs. Among these, film condensation stands out as a commonly observed occurrence. This phenomenon can manifest during natural or forced convection, particularly during rolling motion in ocean-based nuclear reactors. In land-based nuclear reactors, film condensation can occur under static conditions.

The intricate rolling motion observed in ocean conditions generates centrifugal and tangential accelerations [76, 77], impacting heat transfer during condensation. Sun et al. [78] conducted experiments on a C-shaped tube, considering various heat flux levels, rolling periods (0 to 20 seconds), and rolling angles (0° to 15°). Results indicated that rolling significantly influences condensation heat transfer, with up to an 18% increase in the time-averaged heat transfer coefficient at higher rolling angles and frequencies. Further research is needed to explore condensation heat transfer in ocean-based nuclear reactors under rolling motion, an area requiring substantial development.

On the flip side, extensive investigations have been carried out on the transfer of heat during condensation in land-based nuclear reactors, with a specific focus on pressurized water reactors (PWRs) and boiling water reactor (BWR). Generally, these reactors utilize active cooling systems, including fan coolers and containment spray systems, to manage pressure and cool the containment atmosphere. This is achieved by spraying water from the top of the containment structure, whereby falling droplets condense the steam and lower the internal pressure. The latest generation, GENIII+ reactors, uses a passive containment cooling system (PCCS) for long-term cooling and depressurization of the containment building. The PCCS is a passive mechanism that employs natural forces such as gravity, natural circulation, and phase-change heat transfer to remove heat from

the containment [79]. Its primary objective is to withdraw heat from the containment, thereby reducing temperature and pressure. In GENIII+ NPPs, various PCCS designs are employed, including those present in the AP600 [80], AP1000 [2], and other designs ([81–83]). The PCCS system in the AP600 and AP1000 primarily consists of an inner steel containment, a high-water tank spray, and an air loop. The steam condenses on the steel containment tank, transferring heat from within the tank to the outside, and dissipates the condensation heat as air circulates along the exterior of the steel vessel. Despite the presence of NCGs on the condensation side, the steel containment tank features a sufficiently large heat transfer surface area to effectuate adequate heat removal.

On the other hand, certain NPPs, such as HPR1000 [83] and iPOWER [81], have adopted an alternative approach to their PCCS design, unlike plants like AP600 and AP1000. These plants comprise tube-and-shell heat exchangers situated inside the containment structure. An external cooling water tank, strategically located outside the containment structure, interconnects the heat exchangers. Figure 5 depicts this configuration. In the hypothetical scenario at hand, the PCCS circulates water coolant within the tubes through a buoyant flow powered by gravity, driven by the rising temperature of the water. The process of condensation occurs outside the tubes, and the cooling efficiency of the PCCS is dependent on the rate of heat transfer via condensation on the tube's exterior surface as well as the relative arrangement of the tubes and water reservoir. These variables are critical in ensuring the PCCS's cooling functionality under the prevailing conditions [84].

The Economic Simplified Boiling Water Reactor (ESBWR) employs the in-tube cocurrent flow condensation as a passive condenser [52, 85, 86]. This process aids in the transfer of heat from the reactor by allowing steam to condense into the adjacent water pool. Initially, the containment atmosphere is filled with nitrogen. The containment directs the steam-nitrogen mixture to the vertically immersed PCCS condensers, located in a large, interconnected water pool outside and above the containment structure. Within these condenser tubes, steam undergoes condensation, releasing heat into the secondary pool of water. The efficient operation of the PCCS condenser is crucial, as it must extract sufficient energy from the reactor containment to prevent it from exceeding its designed pressure in the event of a design-basis accident.

Moreover, when a NPP undergoes maintenance and refuelling, it is common for the coolant system to be partially drained, which is referred to as a "midloop operation." In this state, the water level of the reactor cooling system (RCS) is above the core but below the elevation of the hot leg [87]. During routine shutdowns and refuelling of a NPP, the residual heat removal system (RHRS) is an active cooling system used to eliminate the decay heat from the core. This system circulates coolant water through the reactor core to prevent it from overheating. In the event of RHRS failure and inadequate cooling for an extended duration, the coolant temperature may rise, eventually reaching its boiling point. This situation can expose the reactor core, ultimately causing fuel cladding failure and damage to the core.

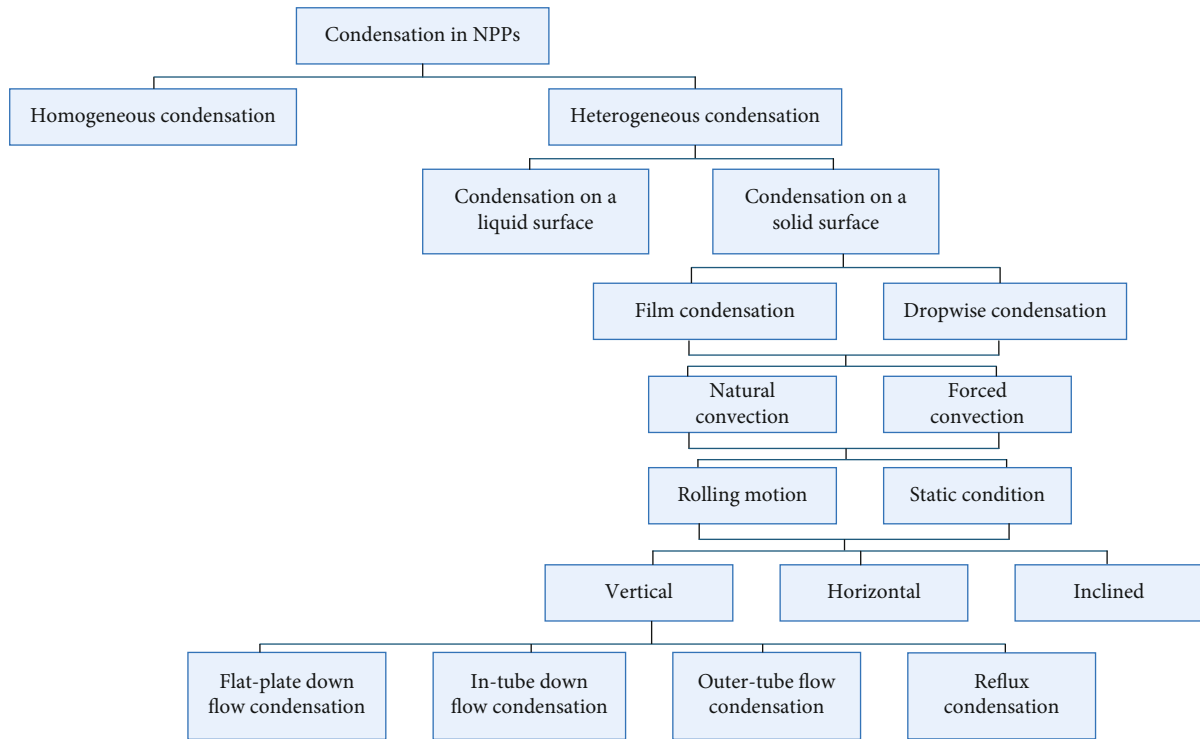


FIGURE 4: Condensation phenomenon classification in NPPs.

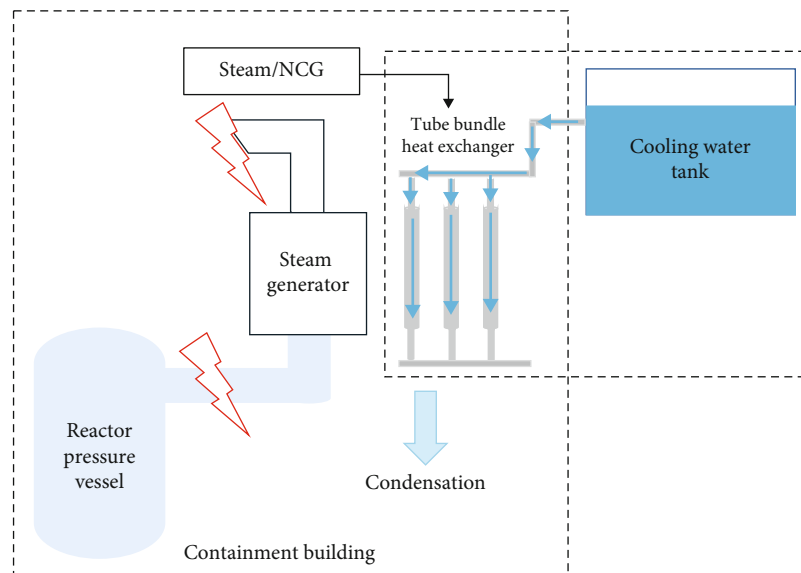


FIGURE 5: Schematic diagram of PCCS.

An approach aimed at mitigating the dissipation of residual heat from the reactor pressure vessel during a shut-down or refuelling scenario may entail employing in-tube countercurrent condensation flow (reflux condensation), thereby facilitating condensation through the hot leg and steam generator tubes. Figure 6 illustrates this technique. Within a natural circulation cooling system, the residual heat present in the reactor coolant prompts the water to boil and generate steam within the reactor pressure vessel. The

resulting steam ascends through the hot leg and flows into the steam generator, where it meets cooler tube walls and releases its thermal energy to the secondary coolant. Following this, the steam undergoes condensation back into water while traversing the cooler tubes of the steam generator and subsequently travels downward to the reactor pressure vessel via the cold leg. The difference in density between hot and cold water powers the establishment of a natural circulation loop. As long as there is a sufficient temperature

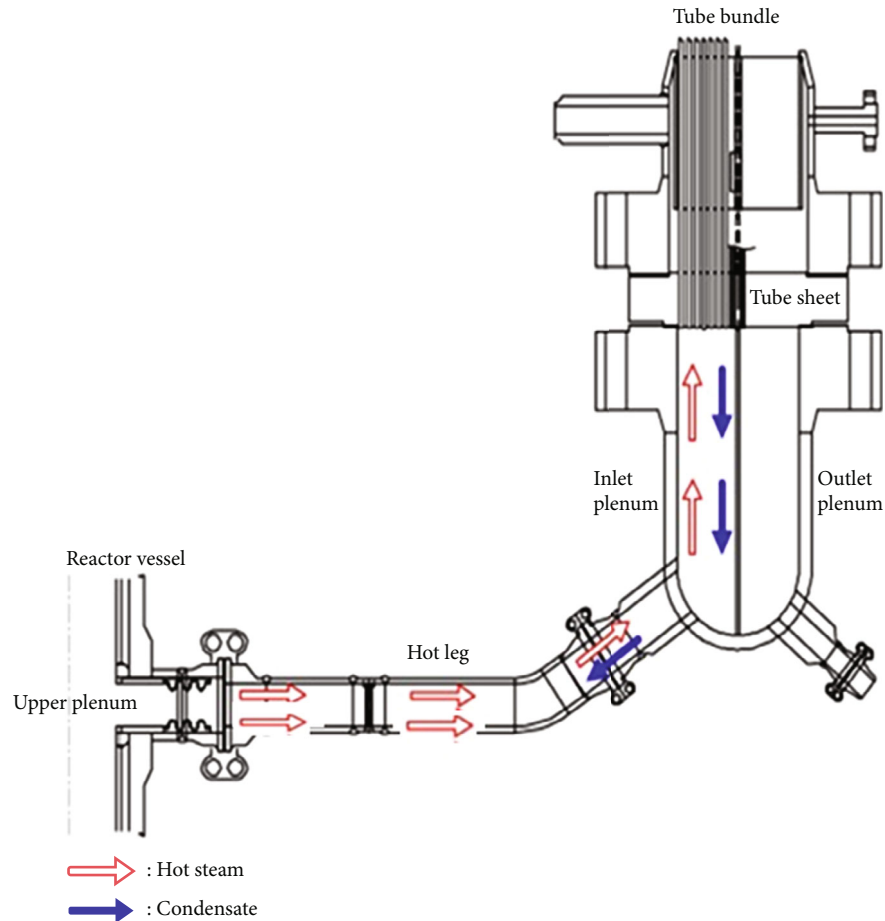


FIGURE 6: Schematic showing the process of reflux condensation that takes place within the steam generator [88] (reused with permission from Elsevier).

differential between the hot and cold sides, this process is capable of extracting decay heat from the reactor pressure vessel and transferring it to the secondary cooling system.

4.2. Condensation in Nuclear Accidents: Natural and Forced Convection. The heat transfer rate through the walls of NPP containment depends on the duration of the accident. Typically, during the early stages of a severe accident, there is a high-temperature gradient, which promotes a uniform condensation process and an increased amount of condensation on the walls. However, despite the higher rate of condensation, there can be a rapid rise in pressure and temperature inside the containment due to the substantial influx of steam during the initial stages of the accident. Figures 7 and 8 demonstrate this phenomenon, showcasing the transient pressure and temperature changes, respectively, within the containment during a MSLB accident at Three Mile Island, which had an energy input of 4800 kJ/m^3 [89]. The effects of this transient pressure and temperature change usually persist for a brief period, lasting between 80 to 120 seconds.

The process of reducing containment pressure and releasing gas during accidents can be divided into two distinct temporal phases, as explained in [90]: the initial blowdown period and the postblowdown period. Through-

out the initial blowdown period, there is a swift escalation in containment pressure and temperature, propelled by vigorous turbulent forced convection condensation. As the rates of steam leakage and condensation approach parity, the pressure and temperature within the containment gradually reach a state of stability, conforming to the prescribed design specifications for the containment system. During the subsequent postblowdown period, the flow undergoes a transition to a less turbulent state, and film condensation, facilitated by natural circulation, primarily governs heat transfer [91]. It is worth noting that several studies examining the thermal-hydraulic behaviour of containment during severe accidents tend to focus solely on the postblowdown period while neglecting the initial blowdown phase. This is primarily due to the intricate and complex nature of the heat and mass transfer dynamics that occur during the initial blowdown period, which pose significant challenges in terms of experimental or computational simulation replication. However, it is crucial to understand the effectiveness of condensation heat transfer during the initial blowdown phase, as it plays a critical role in the overall response of the containment system.

4.3. NCG Sources and Their Transport Perspective in NPPs. In the event of a severe nuclear accident, it is imperative to

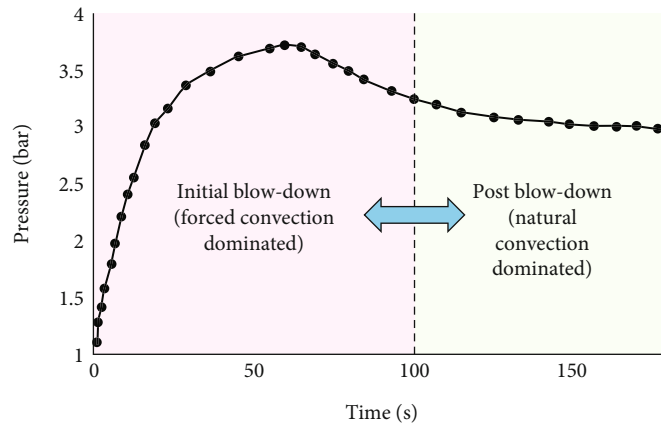


FIGURE 7: Pressure fluctuation caused by a simulated design-basis accident at Three Mile Island, which was triggered by a main steam line break, resulting in an energy input of approximately 4800 kJ/m^3 [89] (reused with permission from Elsevier).

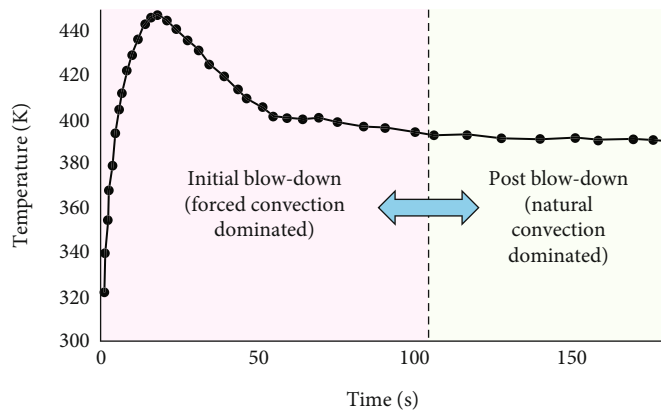


FIGURE 8: Temperature fluctuation caused by a simulated design-basis accident at Three Mile Island, which was triggered by a MSLB, resulting in an energy input of approximately 4800 kJ/m^3 [89] (reused with permission from Elsevier).

comprehend the condensation processes that transpire within the containment area, in the presence of NCGs, to ensure the overall integrity of the containment structure. Steam seeping into an air-filled containment area produces a mixture of steam and air. As the mixture condenses, it becomes denser (with air being heavier than steam) and moves downwards due to gravity, generating a natural circulation pattern and transporting the mixture to the lower part of the containment. As the air layer expands with time, the rate of condensation progressively reduces, thereby necessitating an analysis of the lower containment part to ensure safe peak pressure levels. Over the course of several decades, researchers have conducted a wide range of experimental and computational investigations to explore the complexities of steam condensation in the presence of air. Researchers have meticulously documented and extensively discussed these investigations in [3]. The important reason to study condensation where steam and air exist together is that air could get in, which could threaten the stability and integrity of the reactor vessel and containment. As a result, the nuclear system typically mixes the steam with air before it condenses on a cold surface. Studies have revealed that the steam condensation HTC can decrease by up to 50% when

the air concentration is at 0.5% [4]. Bian et al. [92] conducted a numerical analysis to investigate the thickness of the air layer and its impact on heat transfer. At a distance of approximately 6 mm from the condensation wall, the investigation discerned the thickness of the air layer. This discovery is a strong proof that the layer of air right next to the condensation wall is the main cause of the drop in heat transfer efficiency. These findings are in line with the literature that gases with lower mass diffusivities show larger concentration gradients (see [93]).

On the other hand, in a power plant's normal operation, the reactor containment is filled with nitrogen to maintain an inert environment at a slightly higher pressure than the ambient atmosphere. The gas mixture within the containment comprises mainly air, nitrogen, and steam. However, nitrogen enters the RCS via the accumulator during LOCA. If there is an issue with the accumulator valve following water injection, nitrogen can enter the RCS and lower the efficiency of heat transfer in the steam generator. As the mixture condenses, it becomes denser (air and nitrogen are heavier than steam) and moves downward. In a study conducted by Ma et al. [94], steam condensation was examined within a pressure range spanning from 0.516 to 5.10 MPa

while considering a broad spectrum of nitrogen mass fractions, ranging from 5% to 85%. The results indicated that the condensation HTC decreased from 1.393 to 0.165 kW/(m²•K) at a pressure of 0.517 MPa, and nitrogen mass fractions ranged from 9.03% to 75.76%.

In severe accidents at NPPs, ternary mixtures of light gases, such as helium or hydrogen, may be present. Materials like uranium and plutonium, which are used as fuel in the reactor, primarily produce helium through radioactive decay. During the fission process, the fission process produces and accumulates helium atoms in both the reactor coolant and the fuel itself. An exothermic reaction between steam and zircaloy fuel cladding releases hydrogen gas into the containment area. This reaction occurs at high temperatures (above 1170 K) during zirconium oxidation [95]. Furthermore, as the core meltdown progresses, the likelihood of hydrogen production outside of the reactor vessel increases. For example, the corium can react with concrete, or the containment can be heated directly, as explained in [96]. Therefore, as the mixture condenses, it becomes lighter (helium and hydrogen are lighter than steam) and begins an undesired upward movement. It is important to consider the possible layering of the light gases within the enclosure, where the densities of hydrogen and helium are lower than those of steam, which could lead to stratification. This stratification can cause the condensation HTC in the upper section of the enclosure to decrease by approximately 50% [91]. This occurs because a thick layer of light gases will sit atop a thick layer of steam; therefore, analysis of the containment in the upper part is critical.

Moreover, in the case of a mixture of steam, air, helium, and hydrogen, the direction of upward or downward movement relies on the composition of the mixture in the local region. Consequently, whether steam condensation at a local level promotes natural circulation or stratification depends strongly on the composition of the mixture in that region. This highlights the importance of conducting an analysis at the local level with consideration for pressure and temperature changes and hydrogen management to ensure safe containment operations. If the mixture of steam, air, and hydrogen surpasses the flammable or explosive limit, hydrogen could potentially undergo combustion within the containment [97]. To keep flammable hydrogen from building up at the top of the reactor containment, it is important to be able to predict where it will go during severe accidents [91]. Researchers have mostly undertaken separate studies on steam condensation and hydrogen combustion, despite the closely linked risks associated with these subjects. The challenge of precisely determining the composition of the ternary gas mixture solely through gas temperature measurements contributes to this limitation. Moreover, the integration of experimental inquiries concerning steam condensation and real-time hydrogen combustion is often fraught with difficulties.

Liu et al. [98] discovered that helium decelerated condensation heat transfer by at least 20%. Similarly, Dehbi conducted studies indicating that increasing helium content led to a reduction in heat transfer during condensation [99]. Furthermore, Dehbi suggested an additional 20% decrease

in heat transfer compared to helium, emphasizing that hydrogen has a more detrimental impact on condensation phenomena. In contrast, Paladino et al. [91] reported that the presence of helium had a minimal impact on heat transfer, contrary to the findings of Dehbi and Liu. Additionally, Bucci's research [47] suggested that, for a constant Reynolds number (and thus a consistent Sherwood number), an increase in helium concentration had a positive effect on the condensation rate.

According to [3], when investigating the presence of light gases like hydrogen and helium along with other NCGs, only two factors related to condensation rely on the gas composition, namely, the coefficient $[\alpha D^{2/3}]$ and the driving force of total densities $[\alpha(\rho_b - \rho_i)^{1/3}]$. The addition of a light gas increases diffusion but reduces the driving force by lowering the density of the interface. As a result, these two effects offset each other once the proportion of the light gas reaches a certain threshold. The mass diffusivity of different gas species affects the mass transfer that happens when steam condenses, which in turn affects how the gas concentration is spread across the boundary layer between steam and gas. The concentration gradient of gas species with higher mass diffusivity, such as hydrogen, is less steep than that of those with lower mass diffusivity [93]. Additionally, hydrogen has a low density, which reduces the driving force under natural convection conditions as it decreases the mixture density at the liquid-steam interface. However, it is worth noting that the mass fractions of different species near the condensation wall can have varying gradients due to their higher diffusivity relative to air or steam. Indeed, due to the varying diffusion rates of different gas species, it is essential to solve the transport equations separately for each species. This allows for an accurate representation of individual mass transport behaviour and provides a comprehensive understanding of the diffusion process within the system.

Despite the intimate interconnectedness of the hazards posed by steam condensation and hydrogen combustion, research on these topics has predominantly been conducted in a disconnected manner. The integration of experimental inquiries concerning steam condensation and real-time hydrogen combustion is often fraught with difficulties. To circumvent these obstacles, during investigations into steam condensation, the coupling of combustion analyses can be avoided by utilizing helium as a surrogate NCGs in lieu of hydrogen, owing to safety considerations [9]. The rationale behind this choice can be explicated as follows: the dynamics of gas release and its propagation are governed by five prominent dimensionless parameters, known as the Reynolds number (Re), Schmidt number (Sc), Mach number (Ma), Richardson number (Ri), and density ratio (K). These parameters encapsulate and elucidate the effects of turbulence, diffusion, compressibility, buoyancy, and the ratio of densities, respectively. The physical properties and dimensionless ratios of hydrogen and helium at a pressure of 1 atm and a temperature of 20°C are presented in Table 4. On the basis of these dimensionless ratios, it can be deduced that the decision to employ helium in lieu of hydrogen during experiments is a judicious approach for approximating the local behaviour within the containment [47].

TABLE 4: Physical properties and dimensionless ratios of hydrogen (H_2) and helium (He) at a pressure of 1 atm and a temperature of 20°C.

Parameter	H_2	He
Kinematic viscosity (ν) (m^2/s)	$\sim 1.05 \times 10^{-4}$	$\sim 1.15 \times 10^{-4}$
Diffusion coefficient (D) (m^2/s)	$\sim 6.1 \times 10^{-5}$	$\sim 5.7 \times 10^{-5}$
Sonic speed (V) (m/s)	~ 1300	~ 1000
Density (ρ) (kg/m^3)	~ 0.082	~ 0.164
$\frac{Re_{He}}{Re_H}$		0.91
$\frac{Sc_{He}}{Sc_H}$		1.17
$\frac{Ma_{He}}{Ma_H}$		1.3
$\frac{Ri_{He}}{Ri_H}$		0.46
$\frac{\rho_{He}}{\rho_H}$		2.0

When considering a mixture of steam, air, helium, and hydrogen, the direction of movement, whether upward or downward, is contingent upon the composition of the mixture within the local region, as previously outlined in Section 3.1. Because of this, the effect of steam condensation on natural circulation or stratification at a local level depends a lot on what kinds of things are in the mixture there. The varying concentrations and properties of the gases in the mixture play a crucial role in determining the overall fluid dynamics and the resulting flow patterns in the system. This highlights the importance of conducting an analysis at a local level with consideration for pressure and temperature changes and hydrogen management to ensure safe containment operation.

4.4. Experimental Studies on Condensation Heat Transfer. Researchers have conducted several tests on condensation heat transfer, which can be broadly classified into two categories: separate effect experiments and large-scale experiments. Small-scale experiments in the first group examined the impact of thermal factors, such as pressure, the mass fraction of NCGs, and wall subcooling, on steam condensation. Researchers have performed separate effect experiments to examine the impact of thermal factors, such as pressure, the mass fraction of NCGs, and wall subcooling, on steam condensation. These experiments are documented in references [4, 6, 100, 101]. Large-scale experiments have also been conducted to ensure that safety analysis procedures are accurate and dependable, where the overall behaviour of gas inside the containment following a particular accident is observed. This is essential in validating the numerical codes in real-life accident scenarios. Researchers have conducted large-scale experiments at the TOSQAN [102], THAI [103], and MISTRA [104] facilities.

4.4.1. Separate Effect Experiments. Numerous scholars have embraced a standardized experimental protocol for separate

effect experiments, as depicted in Figure 9. The steam generator with a heater attains the specified steam temperature by applying residual heat generated by the core, causing the heated operational fluid, simulating the reactor coolant, to experience boiling. Within the reactor pressure vessel, the conversion into steam occurs, and it subsequently mixes with a predetermined proportion of NCGs resembling those found in the reactor vessel. The combined mixture flows towards the condensation region, which may be located on a vertical or horizontal wall surface, either inside or outside a tube, where it condenses and transitions into a liquid state. These experiments involve precise measurements of steam flow rate, coolant and surface temperatures, operating pressure, and various other parameters. Researchers then use these measurements to calculate the correlation parameter value. The researchers have developed empirical correlations by employing estimated condensation HTC along with the mass fractions of NCGs and steam. These correlations have gained widespread use in the licensing of nuclear reactor systems. In this study, we present the review of literature on separate effect experiments conducted under different condensation scenarios.

(1) External Wall Condensation. In the past, experimental studies focused mainly on the effect of NCGs on heat transfer during condensation. However, the measurements lacked precision due to the conditions under which they were taken. However, Othmer [4] was the first to address the issue of reduced condensation rates caused by NCGs. Later, Uchida et al. [6] and Tagami [105] conducted the experiments under natural convection on steam condensation in a steel containment with NCGs at a pressure of approximately 1 bar and a temperature of 322 K. The investigation by Al-Diwany and Rose [7] delved into heat transfer measurements for film condensation of steam on a vertical plane surface in the presence of air, argon, neon, and helium under free convection conditions. The results indicate more pronounced reductions in heat transfer for specific noncondensing gas concentrations than previously suggested in earlier reports. Their measurements are consistent with recent boundary layer analyses.

Dehbi [99] did steam condensation experiments to look into how NCGs (such as air, helium, and mixtures of air and helium) affect turbulent natural convection in a vertically oriented condenser tube that has cooling inside it. Dehbi formulated correlations under low-pressure conditions, which predicted heat transfer rates comparable to those deduced from Uchida's [6] experiments. On the other hand, Siddique's experiments have revealed that, for a fixed mass fraction, helium exerts a more inhibiting impact on condensation heat transfer compared to air, whereas air holds greater dominance for the same molar ratio.

Su et al. [106, 107] have performed an experimental examination of film condensation with NCGs, encompassing air and helium, on the external surface of a vertical tube. They utilized an experimental setup comparable to that employed in [99] and investigated a range of parameters, including wall subcooling, total pressure, and NCG mass

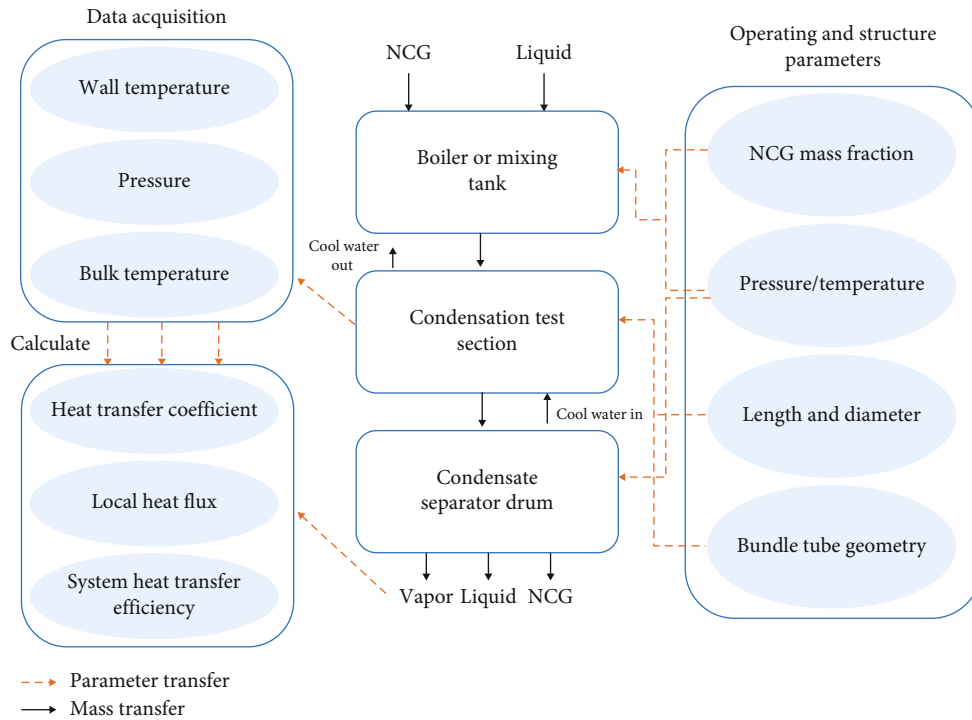


FIGURE 9: Condensation heat transfer tests with NCG flowchart.

fraction. They observed that as wall subcooling increased, the condensation HTC decreased more swiftly. However, the condensation HTC increased with increasing pressure, providing that the NCG fraction remained constant. The outcomes of their inquiry led them to postulate two empirical correlations, one tailored to air and the other relevant to helium and air.

A comparison was made by Su et al. [107] between their experimental observations and three empirical correlations developed by Dehbi [99], Uchida et al. [6], and Liu et al. [98] to assess their practical applicability. Prior to the comparison, the empirical correlations were adjusted using a correction factor. The researchers noted that the predictions of the Uchida et al. [6] and Liu et al. [98] correlations were overestimated by a factor of 2.2 when compared to the experimental data. This discrepancy can be attributed to the significant influence of wall subcooling on the condensation HTC. On the other hand, the Dehbi [99] correlation predicted a condensation HTC lower than the experimental data by up to 20%. Variations in wall subcooling values between the experimental data and the Dehbi correlation could explain this difference. Lee and Park [108] have conducted an inquiry into the behaviour of hydrogen at the local level in a multicompartment mixing chamber. Their study has brought to light that the local test data exhibited a deviation from the widely utilized lumped compartment analysis. These findings have demonstrated the impact of NCGs on steam condensation and underscored the necessity for further research on the parametric study of multicomponent gas mixtures. In a similar vein, Fan et al. [109] have put forth a novel correlation that accurately captures the complex dependencies of condensation HTC on various parameters,

including pressure, air mass fraction, and wall subcooling. The proposed correlation has undergone rigorous validation using experimental data collected by various scholars, thus affirming its applicability not only for steam-air condensation but also for condensation involving steam-nitrogen and steam-argon. The researchers have also underscored that this novel correlation has potential for a vast spectrum of engineering applications, thereby broadening its prospective utility beyond the scenarios probed in their study. Table 5 summarizes the derived empirical equations established by various researchers, outlining the relationship between condensation HTC and operational as well as geometric parameters for condensation on an external tube surface. It is important to note that all these investigations pertain to the natural convection steam condensation.

Several experiments have been conducted to scrutinize the condensation rate in NPPs using diverse passive condenser system designs. However, these experiments have varied in terms of the length and diameter of the wall or tube utilized, as well as the tube bundle geometry, making it crucial to determine the impact of structural parameters on condensation HTC. Researchers have investigated the effects of tube length by placing thermocouples at various locations along the tube. Multiple studies have indicated that the condensation is not notably influenced by the tube length, but there exists an optimal tube length for measuring the condensation HTC [99, 114]. Nevertheless, Lee et al. [116] have discovered that the length of the condenser tube can have a substantial effect on condensation heat transfer under natural convection, as evidenced by their prior research. It has been highlighted that notable variations in the collected data can arise across different facilities, primarily attributed to

TABLE 5: Correlations for condensation heat transfer of steam/NCGs on external surface.

No.	Author (year)	Correlation	Conditions	Geometry
1	Uchida et al. (1964) [6]	$h = 380 \left(\frac{1 - w_{nc}}{w_{nc}} \right)^{0.7}$	$0.23 \leq w_{nc} \leq 0.91$, air	Vertical plate
2	Tagami (1965) [105]	$h = 11.4 + 284 \left(\frac{1 - w_{nc}}{w_{nc}} \right)$	$0.38 \leq w_{nc} \leq 0.83$, air	Vertical plate
3	Kataoka et al. (1992) [110]	$h = 430 \left(\frac{1 - w_{nc}}{w_{nc}} \right)^{0.8}$	$0.5 \leq w_{nc} \leq 0.91$, air	Vertical plate
4	Murase et al. (1993) [111]	$h = 470 \left(\frac{1 - w_{nc}}{w_{nc}} \right)$	$0.46 \leq w_{nc} \leq 0.98$, air	Vertical plate
5	Dehbi (1991) [99]	$h = L^{0.05} [(3.7 + 28.7P_t) - (2438 + 458.3P) \log W_{nc}] \Delta T_{sub}^{-0.25}$	$0.28 \leq w_{nc} \leq 0.9$, $0.15 \leq P_t \leq 0.45$ MPa, $10 \leq \Delta T_{sub} \leq 50$ K, $0.3 < L < 3.5$ m, air/helium	Vertical circular tube
6	Ahn et al. (2007) [112]	$h = [(1381.3 - 85.3P_t) + (2850.3 - 1264.2P_t) \log (W_{nc})] \Delta T_{sub}^{-0.25}$	$0.2 \leq w_{nc} \leq 0.8$, $0.4 \leq P_t \leq 1.2$ MPa, $30 \leq \Delta T_{sub} \leq 50$ K, nitrogen	Vertical circular tube
7	Su et al. (2013) [107]	$h = [(10189.3 + 90416P_t) - (4314.4 + 46537P_t) \log (100W_{nc})] \Delta T_{sub}^{-0.6}$	$0.07 \leq w_{nc} \leq 0.52$, $0.2 \leq P_t \leq 0.6$ MPa, $27 \leq \Delta T_{sub} \leq 70$ K, air/helium	Vertical circular tube
8	Su et al. (2014) [106]	$h = [(-2913.62 + 7957.3P_t) - (7841.62 + 3051.8P_t) \log (W_{nc})] \Delta T_{sub}^{-0.35}$	$0.07 \leq w_{nc} \leq 0.52$, $0.4 \leq P_t \leq 0.6$ MPa, $13 \leq \Delta T_{sub} \leq 25$ K, air/helium	Vertical circular tube
9	Fan et al. (2018) [109]	$h = [(32021 - 22766P_t) + (-16107 + 11736P_t) \log (100W_{nc})] \Delta T_{sub}^{-(0.561 + 0.00134\Delta T_{sub} - 0.546P_t)}$	$0.1 \leq w_{nc} \leq 0.88$, $0.2 \leq P_t \leq 0.5$ MPa, $10 \leq \Delta T_{sub} \leq 70$ K, air	Vertical circular tube
10	Cao et al. (2021) [113]	$h = \frac{0.358(290 + 0.001(L^{1.3}/D^{2.6})) (1 + 0.16 \cos \theta) P_t^{0.6} (w_{nc}/(1 - w_{nc}))^{-0.53}}{(\Delta T_{sub})^{0.05P_t - 0.02w_{nc}/(1 - w_{nc}) - 0.0005\Delta T_{sub} - 0.5}}$	$0.14 \leq w_{nc} \leq 0.87$, $0.15 \leq P_t \leq 1.6$ MPa, $28 \leq \Delta T_{sub} \leq 122$ K, $12 \leq D_h \leq 19$ mm, $0 \leq \theta \leq 90^\circ$, air	Vertical circular tube
11	Liu et al. (2000) [98]	$h = 55.635X_s^{2.344} P_t^{0.252} \Delta T_{sub}^{-0.307}$ $X_s = \frac{W_f/M_s}{W_f/M_s + W_{nc}/M_{nc}}$	$0.1 \leq w_{nc} \leq 0.65$, $4 \leq \Delta T_{sub} \leq 25$ K, $0.25 \leq P_t \leq 0.46$ MPa, $0.395 \leq X_s \leq 0.873$, air/helium	Vertical circular tube
12	Kawakubo et al. (2009) [114]	$h = \min \left[0.33X_{nc}^{-0.8} \Delta T_{sub}^{-0.25}, X_{nc}^{-1} \Delta T_{sub}^{-0.2}, X_{nc}^{-0.25} \right] \times 1000(P_t + 0.5)$	$0.05 \leq W_{nc} \leq 0.5$, $5 \leq \Delta T_{sub} \leq 50$ K, $0.2 \leq P_t \leq 0.5$ MPa, $0.33 < L < 1$ m, $0.05 \leq X_s \leq 0.5$, air	Vertical circular tube
13	Zhang et al. (2021) [115]	$h = \frac{\min \left[0.19X_{nc}^{-1.15} \Delta T_{sub}^{0.2}, X_{nc}^{-1} \Delta T_{sub}^{-0.2}, X_{nc}^{-0.25} \right]}{-0.5705X_{nc}^3 + 0.3395X_{nc}^2 - 0.062X_{nc} + 0.0052}$	$2 \leq \Delta T_{sub} \leq 25$ K, $0.05 \leq X_{nc} \leq 0.3$, $0.1 \leq P_t \leq 0.25$ MPa, air	Vertical circular tube
14	Lee et al. (2017) [116]	$Nu = 890Gr^{0.125} (1 - W_{nc}^{0.01})^{0.966} Ja^{-0.327}$ $Nu = hD_h/kGr = g\beta(\rho_w - \rho_b)L^3/\mu^2$, $Ja = C_p \Delta T_{sub}/h_f g$	$0.1 \leq w_{nc} \leq 0.8$, $19 \leq \Delta T_{sub} \leq 70$ K, $0.2 \leq P_t \leq 0.5$ MPa, $1 < L < 3.5$ m, air	Vertical circular tube
15	Wang et al. (2018) [117]	$h = 1047 \times \frac{P_t^{0.24}}{\Delta T_{sub}^{2.18} W_{nc}^{0.87}}$	$0.05 \leq w_{nc} \leq 0.65$, $0.3 \leq P_t \leq 0.6$ MPa, $5 \leq \Delta T_{sub} \leq 22$ K, air	Vertical circular tube
16	Kang et al. (2021) [118]	$Nu = 14.8 \left(\frac{1 - w_{nc}}{w_{nc}} \right)^{0.37} Ja^{-0.62} Re^{0.39} Ar^{0.2}$ $Re = \rho U_{diffusion} D_h/\mu$, $Ar = L/0.5(D_p - D_h)$	$0.049 \leq w_{nc} \leq 0.89$, $5 \leq \Delta T_{sub} \leq 71$ K, $0.2 \leq P_t \leq 0.6$ MPa, $25 \leq L/D_h \leq 100$, air	Vertical circular tube
17	Jang et al. (2015) [119]	$Nu_D = 1.59 \times 10^{-5} Gr_D^{0.291} Sc^{-19.0} Ja^{-0.744}$	$0.1 \leq w_{nc} \leq 0.8$, $33 \leq \Delta T_{sub} \leq 45$ K, $0.2 \leq P_t \leq 0.4$ MPa, $0.049 \leq v \leq 0.263$ kg*s, air	Vertical circular tube

TABLE 5: Continued.

No.	Author (year)	Correlation	Conditions	Geometry
18	Kim et al. (2020) [120]	$\text{Nu} = 890 \text{Gr}^{0.125} (1 - w_{nc})^{0.966} \text{Ja}^{-0.327} D^* (1 - 1.21 \ln D^*)$ $D^* = D/0.04$	$0.1 \leq w_{nc} \leq 0.8, 0.2 \leq P_t \leq 0.5 \text{ MPa},$ $20 \leq \Delta T_{\text{sub}} \leq 65 \text{ K, air}$	Vertical circular tube
19	Bae et al. (2020) [121]	$h = 0.188 D^{2/3} (\rho_w + \rho_{\infty})^{1/3} \left(\frac{\rho_w - \rho_{\infty}}{\mu} \right)^{1/3} \frac{h_{fg}}{\Delta T_{\text{sub}}} \left[-\ln \left(\frac{1 - w_{s,\infty}}{1 - w_{s,w}} \right) \right]^{0.53} \left(\frac{w_{s,nc} - w_{s,w}}{1 - w_{s,w}} \right)^{0.47}$	$0.09 \leq w_{nc} \leq 0.69, 0.198 \leq P_t \leq 0.503 \text{ MPa},$ $39 \leq \Delta T_{\text{sub}} \leq 65 \text{ K, air}$	Vertical circular tube
20	Dehbi (2016) [122]	$h = \varnothing \cdot \frac{0.13 \rho D (\text{Gr} \cdot \text{Sc})^{1/3}}{L} \cdot \frac{w_{s,\infty} - w_{s,w}}{1 - w_{s,w}} \cdot \frac{h_{fg}}{(T_{\infty} - T_w)}$ where $\varnothing = 1.17 \cdot \Theta = 1.17 (h(1 + B)/B)$ $B \equiv \frac{w_{s,w} - w_{s,\infty}}{1 - w_{s,w}}$	$0.09 \leq w_{nc} \leq 0.38, 1 \leq P_t \leq 4.5 \text{ MPa},$ $5 \leq \Delta T_{\text{sub}} \leq 70 \text{ K, air/helium}$	Vertical flat plate

differences in the overall length of condenser tubes and the aspect ratios of the test vessels. The length of the heat exchange tube and the aspect ratio of the test vessel are critical factors that influence the efficiency of natural convection flow surrounding the condensing surface when a steam-gas mixture is present. Comprehending and taking these factors into account are crucial for guaranteeing accurate and consistent experimental results across diverse facilities.

In a study conducted by Kim et al. [120], an investigation was undertaken to explore the impact of tube diameter on the HTC during condensation. They found that reducing the tube diameter from 40 mm to 21.5 mm resulted in an average increase of 62% in condensation HTC across a range of air mass fractions from 0.1 to 0.8. Furthermore, Dehbi [123] explored the impact of tube curvature and NCGs on condensation in laminar flow regimes. The findings revealed that greater curvature enhanced heat transfer by creating sharper temperature gradients at the tube wall. This resulted in cooler and denser fluid, leading to more pronounced downward convection currents and axial velocities. Consequently, the expulsion of NCGs from the gas-liquid interface was facilitated, thereby enhancing mass transfer and improving the rates of condensation. This mechanism bears resemblance to forced convection, where elevated velocities impede the accumulation of NCGs at the interface, resulting in enhanced condensation rates.

In a study by Wang et al. [117], experiments were conducted to investigate the heat transfer behaviour of both a single tube and a vertical bundle of tubes. They arranged the tube bundle in a single-row configuration to eliminate any potential interference arising from the tube bundle configuration. The study focused specifically on investigating the heat transfer characteristics of mixed gas at high pressure with low mass fractions of NCGs. The results revealed that the tube bundle demonstrated superior heat transfer properties compared to the single tube configuration. Furthermore, the researchers developed a formula to calculate the external condensation HTC of the tube bundle.

In a study conducted by Bae et al. [121] at the CLASSIC facility, an experiment was carried out to scrutinize condensation heat transfer in a genuine PCCS prototype. The experiment revealed that the local HTC of the inner tubes was lower than the average value, primarily due to a shadow effect resulting from the presence of a high mass fraction of NCGs. In another study, Bian et al. [92], it was discovered that variations in tube pitch did not significantly impact the average HTC of tubes on the external surface. However, the heat transfer capacity of tubes located in the center of the bundle was consistently lower than that of a single tube, irrespective of the tube pitch. The researchers ascribed this phenomenon to the fluctuation in local gas flow velocity and the centralized distribution of gas flow, which varied with different tube pitches. It was explained that when the gas flow velocity increased due to a decrease in tube pitch, the NCG layer near the outer surface of the tube diminished, culminating in an increase in heat transfer.

(2) *In-Tube Cocurrent Flow Condensation*. In the context of the Economic Simplified Boiling Water Reactor (ESBWR),

the PCCS utilizes a passive condenser to facilitate the transfer of reactor heat to the surrounding water pool, achieved through the occurrence of steam condensation within the tube. Initially, the containment atmosphere is filled with nitrogen. The steam-nitrogen combination in the containment is then directed downward towards the upper part of the PCCS condensers, which are vertically submerged in a sizable, interconnected water pool positioned outside and above the containment structure. Inside these condenser tubes, steam undergoes condensation, releasing heat into the secondary pool of water. The efficient operation of the PCCS condenser is crucial, as it must extract sufficient energy from the reactor containment to prevent it from exceeding its designed pressure and temperature in the event of a design-basis accident.

Vierow [52] has postulated a method of degradation factor that correlates the calculated cocurrent flow condensation HTC with the Nusselt condensation HTC. Kuhn [124], Lee and Kim [59], and Ađlar and Tanrikut [125] have conducted experiments to explore forced convection steam condensation heat transfer with NCGs inside a vertically oriented condenser tube that features jacket cooling. Kuhn [124] improved the experimental setup by reducing turbulence changes and flow entrance effects. The results were in line with what the theory said would happen. Lee and Kim [59] investigated the local condensation HTC in the presence of NCGs, specifically nitrogen gas, inside a vertical tube. Their research showed that the local condensation HTC goes up when there is more incoming steam and fewer incoming nitrogen gas mass fractions in condenser tubes with smaller diameters. Additionally, their study showed that the local condensation HTC of pure steam and a steam/nitrogen mixture with a low inlet nitrogen gas mass fraction exhibit similar behaviour. Based on what they saw, the researchers came up with a new way to figure out how steam condenses in the presence of NCGs. This new way does not take the tube diameter into account but instead uses interfacial shear strength as a factor. They also noted that the influence of NCGs, particularly nitrogen, on the condensation HTC is less pronounced in smaller-diameter condensers. The proposed correlation demonstrated accurate prediction of the condensation HTC across a range of tube diameters from 1/2 inch to 2 inches. In contrast, the studies conducted by Ađlar and Tanrikut [125] did not account for film waviness due to the low Schmidt number of the air-steam mixture.

Estimations of the HTC during the condensation process within a vertical tube are approached through two distinct correlation types. In the first type, the local HTC takes the form of a degradation factor, representing the ratio of the experimental HTC (when NCG is present) to the pure steam HTC. These correlations generally rely on the local NCG mass fraction and either the mixture Reynolds number or the condensate Reynolds number. The second type of correlation expresses the local HTC using dimensionless numbers. The correlations within this category formulate the local Nusselt number as a function that incorporates the mixture Reynolds number, Jacob number, NCG mass fraction, condensate Reynolds number, and other relevant

parameters. In Table 6, you can see the real-world relationships for HTC when there is cocurrent flow condensation in a tube and NCG is present with forced convection in the secondary loop.

It is important to note that prior research has predominantly concentrated on investigating condensation heat transfer under saturated steam temperature conditions. However, the evaluation of thermal hydraulics during severe accidents requires attention to condensation from a mixture of superheated steam and NCGs. Unfortunately, there has been limited discussion due to the scarcity of data for superheated conditions in most condensation scenarios. In a recent study, Murase and Utanohara [131] conducted a numerical simulation of a prior experiment [132] involving a superheated steam-air mixture in a vertical pipe (49.5 mm diameter) using the CFD code FLUENT. They obtained profiles for mixture temperature, steam mass fraction, and saturated steam temperature, evaluating the applicability of existing condensation heat transfer correlations [128]. The findings verified the reliability of the correlation for evaluating condensation heat flux using the steam mass fraction gradient. Profiles of dimensionless velocity, temperature, and steam mass fraction were obtained and compared with wall functions. The comparison revealed agreement with the linear function in the viscous sublayer and relatively good agreement with the logarithmic law in the turbulent layer, especially in the turbulent layer region under saturated steam-air conditions.

(3) In-Tube Countercurrent Flow Condensation. During accidents or midloop operation in a PWR, there is a potential occurrence of in-tube countercurrent flow condensation (reflux condensation) in the SG tubes. In this situation, instead of water, the SG tubes are filled with either steam or a mixture of steam and NCG. The generated hot steam from decay heat moves upward to the SG tube bundle despite the partial submersion of the reactor core. Some of it condenses and returns to the reactor core, establishing a countercurrent flow of gas and liquid in both the reactor's hot leg and SG. High pressures of 4 to 10 MPa can cause reflux condensation. This can happen because of a LOCA during normal plant operation [133] or at containment pressures resulting from the loss of the RHRS during midloop inventory operations [134].

During the cooling process of reflux condensation in a SG's U-tubes, three distinct modes may manifest depending on operational conditions. A filmwise reflux condensation mode appears initially, characterized by a vertical countercurrent flow of steam and condensate in the upflow section of the U-tubes. After that, the oscillatory mode, which is also called total reflux condensation, starts to show up when the reactor's main coolant drops. This is because a column of one-phase liquid is blocking the riser section above the two-phase region. The natural circulation mode, or carry-over mode, occurs when the liquid column is transported to the opposite side of the U-tube and steam and condensate flow concurrently [135]. Finding the mechanism that controls heat transfer in the U-tubes of SGs is very important when looking at the safety aspects of nuclear power plant safety analyses in the context of reflux condensation.

Al-Shammari et al. [136] conducted an experimental investigation focusing on the film condensation of pure steam and steam in the presence of NCGs within a vertical tube. The study's findings indicated that NCGs had an impact on the resistance to heat and mass transfer in the gas phase during the condensation process. Researchers observed a relatively low resistance to heat transfer on the gas side in experiments involving only steam, with the primary resistance attributed to the condensate film. However, in experiments with steam-NCG mixtures, particularly towards the top of the tube, this resistance experienced a significant increase. This suggests that the presence of NCGs introduces additional resistance to heat transfer in the gas phase during the film condensation process.

Liao et al. [137] employed the heat and mass transfer analogy method in their investigation. They made a mechanistic model that specifically shows how flowing vapor condenses in a reflux process, considering gases that do not condense. The shear stress in their model was quantified through the vapor and film Reynolds number. Pan [138] formulated a mathematical model addressing condensation heat transfer, incorporating factors like mass transfer, vapor velocity, and interfacial shear. The numerical outcomes were then presented, leading Pan to the conclusion that particular attention should be given to the influence of interfacial shear, especially in scenarios involving upward water vapor flow. It is noteworthy that Pan [138] observed Nusselt numbers lower than those anticipated by the Nusselt theory.

Gross et al. [139, 140] explored condensation heat transfer, examining the impacts of film Reynolds and Prandtl numbers as well as interfacial shear stress. In their study [139], some experimental data points for Nu at $Re_f < 10$ were notably lower than the Nusselt prediction. Additionally, Gross et al. [141] conducted a visual investigation into the formation, structure, and frequency of condensate film waves, along with their correlation to the film Reynolds number and shear stress. Lee et al. [142] examined the localized condensation heat transfer under conditions with and without NCG. Furthermore, the current investigation seeks to quantify the impact of SG secondary side pool temperature, as well as the flow rates of steam and NCG (such as air), on the heat transfer phenomenon. The findings indicate that, under conditions of pure steam flow, the local condensation HTCs exhibit stability, maintaining a consistent value of approximately $7500 \text{ W/m}^2 \cdot \text{K}$ along the tube's axial direction. The only exception occurs at low condensate Reynolds numbers ($Re_f < 75$), with this pattern holding steady regardless of changes in steam flow rate and pool temperature. Generally, the obtained results generally agreed with the Nusselt prediction.

Moon et al. [143] and Vierow et al. [144] investigated the local HTCs in the context of reflux condensation. They employed a method that utilized a single vertical tube surrounded by a concentric coolant jacket, promoting a forced convection flow regime. Nevertheless, when the SG U-tubes operate in midloop, the heat transfer conditions on the secondary side shift to natural convection or pool boiling. This shift implies that the presence of the coolant jacket might have an impact on the heat transfer phenomena.

TABLE 6: Empirical correlations for HTC during cocurrent flow condensation inside a tube in the presence of NCG (forced convection in the secondary loop).

Authors	Empirical correlations
Kuhn [124]	<p>For air: $f = f_1 \cdot f_2$ $f_1 = f_{1_shear} (1 + 7.32 \times 10^{-4} Re_f), f_{1_shear} = \frac{\delta_{Nu}}{\delta_{shear}}$ $f_2 = (1 - 2.601 w_{air}^{0.708})$ for $w_{air} < 0.1$ $f_2 = (1 - w_{air}^{0.292})$ for $w_{air} > 0.1$</p> <p>For helium: $f = f_1 \cdot f_2$ $f_1 = f_{1_shear} (1 + 7.32 \times 10^{-4} Re_f), f_{1_shear} = \frac{\delta_{Nu}}{\delta_{shear}}$ $f_2 = (1 - 35.81 w_{he}^{1.04})$ for $0.003 < w_{air} < 0.01$ $f_2 = (1 - 2.09 w_{he}^{0.457})$ for $0.01 < w_{air} < 0.1$ $f_2 = (1 - w_{he}^{0.292})$ for $w_{air} > 0.1$</p>
Vierow and Schrock [57]	$f = f_1 \cdot f_2 = \left(1 + 2.88 \times 10^{-5} \cdot Re_g^{1.18}\right) \cdot (1 - c \cdot w_{NCG}^b),$ <p>where $b = 1.0$ and $c = 10$ for $w_{NCG} < 0.063$ $b = 0.13$ and $c = 0.938$ for $0.063 < w_{NCG} < 0.63$ $b = 0.22$ and $c = 1.0$ for $0.6 < w_{NCG}$</p>
Park and No [126]	$f = 0.0012 w_{NCG}^{-1.4} Ja^{-0.63} Re_f^{0.24}$ <p>For: $1715 < Re_g < 21,670, 12.4 < Re_f < 633.6, 0.83 < Pr_g < 1.04, 0.111 < W_{NCG} < 0.836, 0.01654 < Ja < 0.07351$</p>
Lee and Kim [59]	$f_{steam/NCG} = \tau_{steam/NCG}^{*0.3124} (1 - 0.964 w_{NCG}^{0.402})$ $\tau_{steam/NCG}^* = \frac{1/2 \rho_{steam/NCG} u_{steam/NCG}^2}{g \rho_f L}$ $f = 16/Re_{steam/NCG}$ $f_{pure} = 0.8247 \tau_{pure}^{*0.3124}$ <p>$0.06 < \tau_{steam/NCG}^* < 46.65, 0.038 < w_{NCG} < 0.814$</p>
Siddique [127]	<p>For Air: $Nu(x) = \frac{h_{tot}(x)D}{k_g} = 1.137 \cdot Re_g^{0.404} w_{air}^{-1.105} Ja^{-0.741}$ $0.1 < w_{air} < 0.95$ $445 < Re_g < 22,700$ $0.004 < Ja < 0.07$</p> <p>For helium: $Nu(x) = 0.537 Re_g^{0.433} w_{NCG}^{-1.249} Ja^{-0.6254}$ $0.02 < w_{He} < 0.52, 300 < Re_g < 11,400, 0.004 < Ja < 0.07$</p>
Araki et al. [128]	$\dot{m}_v = D \frac{2P_{tot} MM}{RT_{avg}} \bullet \frac{\ln(P_{gs}/P_{g,b})}{-\ln(1 - (2/Sh))}$ <p>Where: $Sh = \begin{cases} 3.66 & \text{for } Re < 2,300 \\ 0.023 Re^{0.8} Sc^{1/3} & \text{for } 2,300 < Re < 10^7 \end{cases}$ Then, $h_c = \frac{\dot{m}_v h_{fg}}{T_b - T_s}$</p>
Hasanein et al. [129]	<p>For air: $Nu(x) = 1.279 Re_g^{0.256} w_{air}^{-0.741} Ja^{-0.952}$</p> <p>For helium: $Nu(x) = 2.244 Re_g^{0.161} Sc^{-1.652} Ja^{-1.038}$</p> <p>For mixture of air and helium: $Nu(x) = 1.279 Re_g^{0.256} (1 - 1.681 w_{air}) w_{He}^{0.741} Ja^{-0.952}$</p>
Maheshwari [130]	$Nu(x) = 0.15 Re_f^{0.15} w_{NCG}^{-0.85} Ja^{-0.8} Re_g^{0.5}$ <p>For $0.1 < w_{air} < 0.6, 8000 < Re_g < 22700, 0.005 < Ja < 0.07$</p>

Hassaninejadfarahani [145] devised a numerically comprehensive elliptic coupled model for forced convection reflux condensation. The model that was made correctly predicted the rates of condensation and gave detailed axial changes for things like the local Nusselt number, the interface temperature, the gas mass fraction, the film thickness, the centerline temperature, the velocity, and the film thickness. The findings demonstrated that the observed trends closely match the expected physical behaviour.

Janasz [146] developed and assembled the Precise Reflux Condensation Investigation Setup (PRCISE), a concentric tube condenser featuring a vertical test tube surrounded by a cooling water jacket. The outcomes revealed a pronounced stratification in the test tube for both heavy N_2 and light He gases. In each experiment, three distinct regions within the condensation volume were identified: the pure steam zone at the tube's bottom, followed by an intermediate mixing zone, and finally a noncondensable plug on top. The transitional mixing zone emerged as the focal point for analysis, with its shape and behaviour significantly influenced by the type of NCG present. Light gas resulted in a thin and stable interface, whereas heavy gas led to a diffuse and highly dynamic interface. When a mixture of NCG species was introduced, the properties of the mixing zone exhibited a strong correlation with the composition, smoothly transitioning from characteristic behaviour of pure light gas to that of pure heavy gas.

4.4.2. Large-Scale Experiments. The correlations advanced for condensation HTC in separate effect facilities are typically contrived to tackle specific phenomena or amalgamations of phenomena, as opposed to offering a comprehensive portrayal of all facets. Subsequently, these correlations are integrated into numerical codes to simulate the comprehensive dynamics of the containment system. Conducting numerical analysis of the containment system assumes a crucial role in approximating the distribution of mixtures within it and comprehending the combined impact of various phenomena. However, it is important to recognize that these phenomena are interdependent and can mutually influence each other. Consequently, it is plausible that the anticipated behaviour of the containment, as projected by these numerical codes, may diverge from the actual scenario during severe accidents that exceed acceptable thresholds. This discrepancy arises due to the complex and dynamic nature of severe accidents, which may involve multiple simultaneous phenomena that interact and evolve in ways that are challenging to capture accurately through numerical simulations alone. Therefore, while numerical codes and correlations are valuable tools, it is essential to consider their limitations and exercise caution in interpreting their results in the context of severe accident scenarios. Therefore, it is imperative to validate the numerical codes under realistic accident conditions before employing them for safety analysis and designing future nuclear power plant containments. To accomplish this, large-scale facilities known as integral experimental facilities have been developed to replicate either the entire or partial sequence of a reactor accident.

Table 7 provides examples of large-scale facilities along with the corresponding parameters they consider. Meanwhile,

Table 8 presents an overview of the approximate actual conditions for several key parameters within the reactor containment. It is evident that the parameter range of large-scale facilities aligns with the approximate actual conditions found within the reactor containment. Nevertheless, additional research is required to explore accident scenarios to enhance our understanding in this area. It is important to emphasize that the primary challenge in experimenting with the condensation phenomenon is the significant size of the enclosure and its strong dependency on boundary conditions. These factors necessitate ensuring a strong correlation between the simulation and validation of the model and the faithful replication of flow dynamics occurring inside the containment structure.

4.5. Containment Thermal-Hydraulic Codes. The global initiatives aimed at simulating containment accidents have commenced experimental work in two directions: the separate effect test facility and the large-scale facility. These initiatives seek to overcome the current lack of data on large-scale containment and verify the accuracy of thermal-hydraulic codes capable of simulating three-dimensional containment. However, it should be noted that the experimental work alone has not fully confirmed the reliability of these codes [3]. The utilization of thermal-hydraulic codes for the analysis of containment systems at a local level is prevalent. These codes employ numerical techniques to discretize conservation equations in time and space. They are categorized into lumped parameter (LP) codes or computational fluid dynamics (CFD) codes [149]. LP codes have limitations in accurately predicting time-dependent behaviour within a control volume. These codes also do not account for spatial variations of variables such as density, velocity, concentration, and temperature. To model heat transfer during steam condensation, LP codes typically rely on empirical correlations based on experimental data that has been averaged across the volume. Additionally, each compartment in a containment system is treated as a control volume for solving energy and mass conservation equations, while the momentum equation is solved in one dimension using the flow paths of the control volumes. However, the one-dimensional approach of LP codes is inadequate for accurately predicting certain local-scale phenomena, including momentum advection, mixing, natural circulation, stratification, and combustion. Consequently, these codes can only provide an approximate average estimation [150, 151]. Even though they have their limits, simplified codes like LP codes can make fairly accurate predictions of gas stratification (averaged over a control volume) in typical low-velocity turbulence or laminar conditions, which help natural circulation within the containment system [147]. Thus, these codes are frequently utilized for the analysis of thermal hydraulics within containment facilities and for the assessment of safety probabilities since they can offer average estimations of parameters with moderate computational efforts [149].

CFD codes employ correlations, derived from volume-averaged computations, to solve momentum and energy equations [152]. In CFD simulations, a single-fluid model is employed, treating steam as a separate species through a species conservation equation or by solving separate

TABLE 7: Examples of large-scale facilities and their corresponding parameters.

Experiment Parameter	TOSQAN [147]	THAI [103]	PANDA [148]	MISTRA [148]
Dimension (m)				
Facility	$\varnothing = 1.5$ m $H = 4.8$ m	$\varnothing = 3.2$ m $H = 9.2$ m	$V = 515$ m ³ $H = 25$ m	$\varnothing = 4.25$ m $H = 7.3$ m
Condenser	$\varnothing = 9.4$ $H = 2$ m	—	—	3 units -26.2 m ² , 2 × 21.4 m ² $H = 5$ m
Flow	Natural convection	Natural/forced convection	—	Natural convection
Gas velocity (m/s)	0-6.0	—	—	0-3.5
NCGs				
Type	Air-He	Air-He	Air-He	Air-He
W_{NCG} (%)	15-75	80-95	0-30	—
Pressure (bar)	1-6	1-1.5	10	3-3.5
Temperature (°C)	60-153	20-65	200	120-135
Condensation HTC (W/m ² K)	100-1000	—	—	—
Objective	This facility is utilized to investigate the influence of specific factors, such as pressure, velocity, temperatures, mixture composition, and more, on the rate of condensation and the flow of local species. By manipulating and controlling these factors in experimental setups, researchers can gain insights into the mechanisms and behaviours associated with condensation processes.	This facility is employed to probe interconnected phenomena, encompassing the combined effects of gas injection and the process of condensation, natural circulation and stratification, distribution and the effects of depletion, the distribution of condensate on walls, the creation of fog, and the dynamic thermal response of heat-conducting walls. By scrutinizing these interconnected phenomena in a regulated experimental environment, researchers can acquire insights into the complex dynamics and behaviours that transpire during severe accidents in nuclear reactors.	This facility is employed to reproduce mixing and stratification phenomena observed in scenarios involving the combination of steam with air and steam with helium. It encompasses the sequential injection of steam-helium into an air-filled facility to scrutinize the effects of the concurrent presence of air and helium gas on flow conduct. Additionally, the facility is used to investigate the independent and interconnected impacts of the steam jet on the disruption of stratification. It also allows for studying the influence of safety components and the abrupt opening of hatches that serve as barriers between the two volumes on flow transport. By conducting experiments in this facility, researchers can gain valuable insights into the complex interactions and behaviours of different gases in various scenarios, enhancing our understanding of flow dynamics during severe accidents in nuclear reactors.	The facility is utilized to validate the accuracy of thermal-hydraulic codes on a large scale. It allows researchers to investigate the interactions of various phenomena, such as steam condensation, stratification, turbulence, and buoyancy forces. By comparing the experimental results obtained from the facility with the predictions of the thermal-hydraulic codes, researchers can verify the reliability and accuracy of these codes in simulating and predicting complex thermal-hydraulic behaviours during severe accidents in nuclear reactors.

momentum equations for the steam and gas phases. These equations are solved simultaneously, incorporating sink and source terms to accommodate steam condensation in the mass, momentum, and energy equations. However, it is

important to note that the development of CFD codes involves a significant amount of time and effort. This includes tasks such as developing numerical models, determining appropriate mesh parameters, conducting validation

TABLE 8: Estimate the real conditions within the containment area [3].

Pressure (bar)	NCG mass fraction (%)	Gas velocity (m/s)	Condensation HTC (W/m^2K)
2.48-4.55	30-60	0.3-3	100-1500

exercises, and performing actual computations. These processes can be notably time-intensive, particularly for large-scale facilities akin to containment buildings [153]. In addition, the acquisition of empirical data to authenticate CFD codes poses formidable obstacles owing to the intrinsic perils associated with hydrogen combustion experiments. Furthermore, various factors encompassing the instability of condensate films, splashing phenomena, film rupture occurrences, suction influences, surface attributes, morphological repercussions, and subcontinuum mechanisms elude integration within CFD-based simulations. Consequently, the establishment of thermal-hydraulic codes demands substantial temporal investments, computational resources, and meticulous validation protocols to ascertain their dependability in approximating containment thermal hydraulics.

Both approaches have their advantages and limitations, and the choice between them depends on the specific application and the desired level of detail and accuracy. Table 9 gives a brief overview of the abilities of LP and CFD codes. The use of containment thermal-hydraulic codes for modelling condensation in the presence of NCGs has been extensively studied and validated over the years. These codes can simulate the complex interactions between steam, NCGs, and the containment surfaces and can provide valuable insights into the behaviour of containment structures under accident conditions. However, the accuracy of the results obtained from these codes depends on several factors, including the quality of the input data, the modelling assumptions, and the numerical algorithms used. Therefore, it is important to carefully evaluate the uncertainties and limitations associated with the use of these codes and to perform sensitivity analyses to assess the impact of different modelling choices on the results.

Moreover, LP and CFD codes both employ either a HMTA model or correlations derived from experiments to estimate condensation heat transfer. Table 10 presents a compilation of various LP and CFD codes that have been developed, along with the condensation models used in each code. Since typical CFD software does not typically deal with changes in state, it is essential to create and confirm accurate models within the CFD software that consider the reduction of mass, momentum, and energy that results from condensation. Martín-Valdepeñas et al. [97] have initiated efforts to achieve this objective, but their model implementation in the CFX-4 software was based partly on empirical correlations.

Houkema et al. [155] utilized custom subroutines within the CFX-4 CFD software to model condensation with NCGs present, employing the standard Stefan flow equation. The study showed reasonably accurate results for low condensation rates; however, the model failed to account for the higher rates of condensation, which are known to increase mass transfer beyond levels predicted by the Stefan flow

equation. The model did not contain provisions to adjust for these higher rates. Dehbi et al. [156] used a model based on fundamental principles in the ANSYS CFD software Fluent to anticipate wall condensation in the presence of steam and NCGs. Their results demonstrated excellent agreement between calculated heat transfer rates and existing analytical solutions and experimental correlations.

On the one hand, to evaluate nuclear safety containment codes, the international standard problem ISP47 was arranged [147]. There are multiple test facilities that are affiliated with ISP47, and one such facility is the CEA MISTRA facility [70]. The MISTRA facility's experimentation involving the combination of air and water steam in the existence of cold walls and steam condensation was the focus of ISP47 [70, 71]. The majority of the assessment of the MISTRA ISP47 trial was executed using codes that employed lumped parameters [70]. In various analytical experiments, CFD calculations were frequently employed, as demonstrated by the studies of [72]. Punetha and Khandekar [157] went even further by extending the use of CFD to the small-scale TOSQAN facility nestled within IRSN. CFD has been utilized for smaller containment structures, but limited information is available regarding larger containment structures such as the 97.6 m³ MISRA containment. Recently, two CFD code developments based on OpenFOAM have been reported. Kim et al. [158] conducted an analysis of the hydrogen distribution within an OPR1000 containment; however, details regarding the equations used or the validation of the code were not included. On the other hand, Kelm et al. [159] described the development and validation strategy of their CFD code, containmentFOAM, which can implement wall condensation through either a volume source term or wall fluxes. In addition to handling turbulent mixing and water steam condensation, containmentFOAM also considers radiative heat exchange and aerosol transport. Preliminary validation results were presented, and areas for future research were identified. ContainmentFOAM encapsulates the complete gamut of physical elements related to species transportation and homogeneous and wall condensation.

5. Recent Advances in Steam Condensation Heat Transfer Research

Given this extensive examination of steam condensation in the context of NCGs for NPP applications, it is essential to underscore existing gaps in knowledge and outline future research goals. Therefore, the forthcoming sections will spotlight various subjects that the authors consider potential breakthroughs or achievements that should shape the trajectory of future research endeavours.

5.1. Wall Condensation Model for CFD Application. As previously discussed in Section 4.1, steam condensation on containment structures serves as a crucial heat transfer mechanism during LOCAs in NPPs. This process plays a pivotal role in limiting the pressurization of the containment and influences the effectiveness of safety measures like the containment cooling system. Additionally, the condensation on walls diminishes the steam concentration in the containment atmosphere, thereby impacting the flammability of the

TABLE 9: Assessing the respective capabilities of LP and CFD codes [149, 154].

Parameter	LP codes	CFD codes
Computational time	Relatively fast running	Long computational time
Number of nodes	Adequate (≈ 100 control volumes)	Fine (≈ 105 cells, cell size $\approx 10^{-11}$ m ³)
Input parameter	Modest	Local data input required at each cell
Validation	Large validation base available	Limited
Parametric study	Feasible due to fast computing	Limited due to long computational time
Predicting flow paths	Adequate for sufficient nodes	Well predicted

TABLE 10: The thermal-hydraulic codes incorporate various condensation models [3, 154].

No.	Abbreviation	Type	Condensation model
1	GOTHIC	LP/CFD	Uchida correlation and Gido and Koestel correlation (HMTD)
2	COCOSYS	LP	Stefan law (HMTA)
	ASTEC	LP	
	CONTAIN	LP	
3	PCCSAC	CFD	Collier's model (HMTA)
	CONTEMPT-LT	LP	
	COMMIX-1D	CFD	
4	MAAP-DBA	LP	Uchida and Tagami correlations
	COMPACT	LP	
5	GASFLOW	CFD	Chilton-Colburn analogy (HMTA)
6	CONTEMPT-4/MOD5	LP	Tagami correlations and other
7	MELCOR	LP	Collier's mass flux and Chilton-Colburn correlation (HMTA)
8	TONUS	LP/CFD	Chilton/Bird condensate rate formulation with McAdams correlation (HMTA)
9	RELAP	LP	Colburn-Hougen model (HMTA)
10	CFX-4	CFD	Nonimplemented
	FLUENT	CFD	

hydrogen-steam-air mixture. Consequently, wall condensation holds significant importance in maintaining the integrity of the containment, serving as the ultimate barrier against the release of hazardous radioactive materials into the external environment. Hence, there is an urgent requirement for both experimental and numerical investigations concentrating on wall condensation. In the realm of safety assessment, the exploration of three-dimensional phenomena and localized effects has sparked the integration of CFD to enhance our understanding of containment atmosphere mixing, serving as a valuable supplement to established system codes. Consequently, the crucial necessity for an accurate representation of wall condensation emerges to guarantee the effectiveness of CFD applications. However, the practical challenges associated with implementing such extensive applications underscore the need for a numerically efficient and robust model.

The TOSQAN experimental program, as outlined by Malet et al. [147], was developed to replicate the thermal-hydraulic flow conditions typical of accidental scenarios within a reactor containment. Investigating the heat and mass exchanges between spray droplets and gas under thermal-hydraulic conditions representative of hypothetical severe accidents was explored in the study conducted by

Mimouni et al. [160]. Cheng et al. [101] examined condensation over a vertical plate measuring 2 meters in height and 0.6 meters in width, positioned within a rectangular channel with a depth of 0.5 meters. The plate's rear surface was cooled by water at a consistent temperature, varying pressure, air mass fraction, and velocities. The study placed particular emphasis on its relevance to reactor containment during severe accident conditions, highlighting the demonstrated impacts of gas concentration, gas velocity, and surface inclination on condensation heat transfer.

Bucci [47] explored a broader spectrum of phenomena associated with the existence of NCGs lighter than steam in a test section. This section, approximately 2 meters long with a square cross-section measuring 0.34 meters on each side, circulated a mixture of steam, air, and helium. The primary objective was to enhance comprehension of the impacts caused by helium, particularly in relation to buoyancy forces. The study presented new data by examining cases with low free stream velocities.

Dehbi et al. [156] incorporated a model for wall condensation from a vapor-NCG mixture into the ANSYS CFD code Fluent. They introduce volumetric source (sink) terms in the control volumes neighboring the wall. The predicted heat transfer rates exhibit overall good agreement with

existing analytical solutions and experimental correlations. Zschaeck et al. [161], utilizing the ANSYS CFX commercial CFD package, address the condensation of steam in the presence of air by incorporating a mass sink at isothermal walls or interfaces within the conjugate heat transfer domain where condensation occurs. Validation of the model was conducted using the data presented by Ambrosini et al. [162] and Kuhn et al. [58]. In a recent study, Kumar et al. [163] extensively discuss a CFD model designed for predicting vapor film condensation on walls in the presence of NCGs. The model was formulated within the containment-FOAM solver framework, utilizing the open-source CFD code OpenFOAM. The primary application focus was on simulating the mixing of the nuclear reactor containment atmosphere. The authors validated the model by comparing it with experimental data from the SETCOM facility, specifically for flows in the forced convection regime. The results indicated favourable agreement between the model predictions and experimental data, encompassing total wall fluxes across three cases with varying condensation rates. This agreement held true for both fine and coarse meshes.

In summary, these advancements create opportunities for in-depth investigations into natural and forced convection flows, specifically within the mixed convection regime expected in the containment during the prolonged phase of an accident transient. Furthermore, there is a critical need for the validation of models through diverse separate effect tests and large-scale experiments that are pertinent to real-world applications. This validation is essential not only to refine and enhance the models but also to discern their limitations.

5.2. Multiscale Simulation of Wall Film Condensation Using Coupled CFD and System Analysis Codes. Typically, when calculating the cooling of a mixture of gas and steam, it is assumed that the temperature at the wall remains constant and that the heat flux or temperature profile remains unchanged. However, when dealing with condensers, the temperature or heat flux is not always predetermined, unless the cooling water's mass flow rate is significantly higher than that of the gas-steam mixture or the water-steam mass fraction in the gas-steam mixture is low [47]. Therefore, it is more efficient to consider both the heat transfer that occurs in the cooling water and the heat transfer caused by gas-steam condensation. To address this issue, Li [164] pioneered a technique contemplating the heat transfer inherent in a cooling jacket, and the results garnered bore a satisfactory resemblance to the empirical data without necessitating conjectures regarding the condenser wall's thermal state. Analogously, Zschaeck et al. [161] incorporated a depiction of the cooling conduit within their modelled condensation scenario.

In order to secure an authentic assessment of the PCCS's efficiency and the containment's fortitude, it becomes paramount to scrutinize not only the condensation process but also the natural circulation, which involves boiling occurring within the heat exchanger tubes. For the determination of the cooling system's ability to uphold its projected cooling potential for a substantial duration approximating 72 hours,

it becomes necessary to implement an enduring transient scenario simulation inclusive of a biphasic examination of natural circulation. However, undertaking a comprehensive CFD analysis of the entire system, encompassing both the cooling and containment aspects, presents formidable computational and analytical challenges due to the biphasic nature of the natural circulation study and the prolonged transient simulations involved [165]. To overcome this obstacle in a practical fashion, a multiscale analytical methodology has been suggested, which involves the combination of the nuclear reactor safety analysis code with a specialized CFD code designed for analyzing the behaviour of the heat exchanger tube. This fusion of codes could be interpreted as a multiscale approach since the nuclear reactor analysis code is typically engaged for system-level evaluations, whereas the CFD code is harnessed for localized assessments [165]. The integration of CFD codes, which offer detailed data, with system analysis codes, which provide a panoramic outlook, equips researchers and engineers to attain insights into the system's behaviour that would be challenging to acquire using either method in isolation.

In the field of nuclear engineering, there are integrated codes that have been applied, including the CUPID [166] and MARS [167] codes. MARS manifests a one-dimensional lattice of conduits that has been validated against an expansive experimental database, inclusive of biphasic conditions, and can be utilized to simulate fluid kinetics within pipes and heat exchanger tubes. In stark juxtaposition, for emulating the shell-side phenomena, one can harness CUPID, a multidimensional biphasic flow analysis code developed at the Korea Atomic Energy Research Institute. Given that shell-side phenomena boast multidimensional characteristics, a synchronized simulation methodology proves practical in proffering adequate boundary conditions for the temperature distribution across the heat exchanger wall while safeguarding the accuracy of heat transference predictions.

The study of wall film condensation in nuclear engineering is a fresh and challenging research field. It involves simulating condensation processes on various scales, which is a complex task requiring sophisticated methods. To the best of the author's knowledge, there have been few investigations conducted in this particular field [165, 168, 169] emphasizing the need for more extensive research. Through further investigations, we can improve our understanding of wall film condensation and advance the development of modelling techniques. These advancements would have significant implications for the design of heat transfer systems in the nuclear industry, offering substantial benefits.

5.3. Steam Condensation Heat Transfer Based on Machine Learning (ML) Models. As we continue to rely on nuclear energy as a source of power, it becomes increasingly important to ensure that our NPPs operate safely and efficiently. As mentioned earlier, one of the key challenges facing the nuclear industry is the phenomenon of condensation in the presence of NCGs. This process is complex and involves the interaction of various physical variables, making it challenging to model accurately using conventional analytical, experimental, and numerical techniques.

Soft computing approaches in ML algorithms can help researchers and engineers better comprehend the underlying dynamics of condensation in the presence of NCGs. These approaches can analyze large volumes of data from experiments and simulations, identifying patterns and relationships that are difficult or impossible to detect through traditional methods. Leveraging ML to model condensation in NPPs has enormous potential benefits. Engineers can optimize reactor design and operation by developing more accurate predictive models, ensuring safety, and maximizing efficiency. Additionally, gaining a better understanding of the underlying physics of this process can aid in managing the risks associated with the plant operation and ensuring that it remains a reliable and sustainable energy source for future generations.

Researchers have gathered numerous datasets over time while examining flow condensation heat transfer with varying fluids and geometric and flow parameters. By utilizing advanced ML models, it is now feasible to identify the connections between these input parameters and their respective significance in determining the output parameters [170]. For instance, Zhou et al. [171] investigated the flow condensation heat transfer in mini/microchannels using a database of 4,882 data points. The researchers employed four ML models, including artificial neural network (ANNs), random forest, adaptive boosting, and XGBoost. The team found that the ANN model had the best prediction accuracy, with a mean absolute error (MAE) of 6.8%. Another study by Zhu et al. [172] collected data on the flow, boiling, and condensation of refrigerant R134a in two miniature channels with serrated fins under varying operating conditions. This research contrived ANN models that offered HTC estimations with mean absolute relative difference of 11.41% and 6.06% for boiling and condensation, respectively, upon comparison with experimental data.

Balcilar et al. [173] embarked on an exploration of the condensation HTC and pressure deviations of R134a in a diminutive vertical tube, employing an array of ANN methodologies such as the multilayer perceptron (MLP), radial basis function networks (RBFN), generalized regression neural networks, and an adaptive neuro-fuzzy inference scheme. The investigators discerned that, save for a minor aberration, the MLP procedure possessing a 5-13-1 architecture, in conjunction with RBFN, exhibited strong agreement with the empirical data. On a different note, Azizi and Ahmadloo [174] engaged an ANN built on 440 experimental data pieces to scrutinize the condensation HTC in a sloped tube, registering a MAE that fell below 2%.

Cho et al. [175] utilized ML models to forecast the rate of condensation heat transfer. They used a MLP neural network model and found that it outperformed previous correlations with a MAE of 4.2%. They subsequently presented the prediction model they developed in the given correlation.

$$h = 3.18 \left(\frac{L}{D_h} \right)^{0.1} \left(\frac{w_{nc}}{1 - w_{nc}} \right)^{-0.47} (P_s)^{0.51} (\Delta T_{sub})^{-0.34}. \quad (48)$$

In this context, the units for L , D_h , P_s , and ΔT_{sub} are meters (m), millimetres (mm), megapascals (MPa), and

kelvins (K), respectively. It is noteworthy to mention that this correlation and the subsequent developments were derived from normalized data, with variations specific to each respective study.

The accuracy of Cho et al.'s correlation was evaluated in a thorough manner using a total of eight correlations derived from experiments that did not consider geometric parameters, along with an additional four correlations that did consider them, presented in Table 5. Among the correlations that did not factor in geometric parameters, Su et al. [106] yielded the most accurate predictions with a MAE of 23.0%. In contrast, Dehbi's [99] correlation, which did take into account these parameters, exhibited the greatest accuracy, registering a MAE of 13.0%.

Similarly, Lee et al. [176] leveraged a CNN-based DenseNet framework and discovered that their machine learning prototype boasted a prediction prowess surpassing that of existing correlations. Lee et al. [176] generated 3,000 pseudo data points, utilizing a group of ten established condensation models as their foundation for crafting their neural network model. This model was an intricate blend of a fully interconnected layer and a DenseNet structured on convolutional neural networks. Their model underwent rigorous validation via the process of holdout cross-validation before facing examination against experimental data not part of the initial training set. The conclusions revealed the neural network model's extraordinary aptitude in predicting condensation HTC, largely due to its successful acquisition of the strengths ingrained in each correlation. Considering the parametric analysis outcomes, a fresh empirical correlation was proposed, taking into account the impacts of the pertinent variables. The prediction model they meticulously engineered was later displayed in the provided correlation.

$$h = \frac{L^{0.347} [(-0.542 + 0.00085P_{tot}) - (18.8 + 0.0354P_{tot}) \log_{10}(w_{NCG})]}{D_h^{1.356} (\Delta T_{sub}/T_{cr})^{[(0.351+0.0488w_{nc})(1-(T_{crit}/\Delta T_{sub}))-(29.97/P_{tot})]}},$$

$$T_{cr} = 1889.35P_{tot}^{1.072} w_{NCG}^{0.322} D_h^{3.587}. \quad (49)$$

In this context, the units for L , D_h , P_{tot} , and ΔT_{sub} are meters (m), millimetres (mm), megapascals (MPa), and kelvins (K), respectively.

The newly developed correlation was assessed against the correlations derived from the experimental data in Table 5. Of these correlations, Jang et al. [119] offered the most precise forecasts, with a MAE of 9.8%.

In a recent study by Alboudour et al. [177], they employed a predictive MLP network to analyze vertical tubes in the presence of noncondensable and light gases. The study utilized extensive databases containing diverse inputs for passive containment cooling systems in NPPs. A novel correlation for condensation heat transfer coefficient was formulated and assessed. The newly developed correlation demonstrated exceptional accuracy in predicting condensation HTC, highlighting its effectiveness.

The ML methods used in previous studies pose challenges in terms of visualizing and expressing the mathematical relationship between inputs and outputs. Additionally,

these models are not easily transferable to other analysis codes. To address these limitations, genetic programming (GP) can be used to generate simplified prediction expressions that offer a solution to these issues [178, 179]. Multigene genetic programming (MGGP) constitutes a fresh advancement in GP that amalgamates shallow-depth GP modules linearly to elevate the accuracy of resolutions [180]. The model that MGGP develops boasts a reduced complexity in contrast to monolithic GP, primarily attributable to the employment of more compact trees [180]. Moreover, MGGP necessitates a lesser quantity of training data in comparison to other models, and the ensuing compact and lucid models can be immediately leveraged in other safety simulation codes.

In a recent study, Tang et al. [181] employed an MGGP model to forge new correlations for ascertaining the condensation HTC of steam-NCG mixtures over a vertical conduit under turbulent free convection circumstances. They assembled an exhaustive dataset consisting of 1,440 data entries from 18 sources to construct both a novel empirical correlation and an MGGP model for an enhanced juxtaposition. The outcomes of their research illustrated that the MGGP method is a promising technique to develop precise, reliable, and concise models for intricate heat transfer and multiphase flow phenomena, specifically addressing steam condensation in the presence of NCGs. Tang et al. [181] formulated three predictive models that were subsequently demonstrated in the following correlations.

$$h = 111 \left(\frac{w_{nc}}{1 - w_{nc}} \right)^{-1} + 888, \quad (50)$$

$$h = 977 \left(\frac{w_{nc}}{1 - w_{nc}} \right)^{-0.5} - 188, \quad (51)$$

$$h = \left[4.00P_v^{0.5} \Delta T_{sub}^{-0.5} - 3.952P_s^{0.5} D_h + 3.691 \times 10^2 \right] \left(\frac{w_{nc}}{1 - w_{nc}} \right)^{-0.5} + \frac{2.474P_s D_h - 5.761 \times 10^5 D_h^3 P_v^{0.5}}{\Delta T_{sub}} - 68.380, \quad (52)$$

where the units for D_h , P_v , and ΔT_{sub} are millimetres (mm), megapascals (MPa), and kelvins (K), respectively.

Interestingly, in the most straightforward MGGP correlations delineated in Equations (50)–(52) the condensation HTC is solely determined by the ratio $w_{nc}/(1 - w_{nc})$. This is identical to the simplest empirical correlations advanced by Uchida et al. [6], Tagami [105], Kataoka et al. [110], and Murase et al. [111]. The correlations extrapolated from experimental data were contrasted with the condensation HTC as prophesied by the third correlation. The correlation based on the MGGP approach was found to exhibit superior accuracy and minimal discrepancies in predicting the condensation HTC compared to the majority of the other correlations. Additionally, the third correlation was assessed against the correlation derived from the ML endeavours of Cho et al. [175]. Tang's correlation outshone Cho's

correlation, with a MAE of 14.8%, while Cho's MAE stood at 17.5%.

In conclusion, the current ML techniques used for condensation heat transfer have exhibited promising results, paving the way for a brighter future in this field. These methods have demonstrated their ability to accurately predict condensation rates and identify optimal operating conditions for efficient condensation, leading to enhanced process performance. However, the need for further investigation remains to fully understand the complex behaviour of condensation in the presence of NCGs and to explore the potential of integrating these techniques with other technologies for enhanced process control and optimization. With the ongoing research and development, ML can undoubtedly provide a powerful tool for improving condensation processes.

6. Concluding Remarks: Prospects and Recommendations

This review provides a trajectory for future research by studying the intricacies of steam condensation, especially in the presence of NCGs, which can hinder the safety and optimal functioning of nuclear reactors. The conclusions drawn from this review are presented below:

- (i) Recent studies highlight the considerable difficulties presented by even small quantities of noncondensable gases (NCGs) in the process of steam condensation. Although previous research has delved into steam condensation involving air and touched upon nitrogen, there are persisting gaps in knowledge, particularly concerning ternary mixtures that include light gases such as helium or hydrogen resulting from accidents in nuclear power plants (NPPs) in the presence of steam; the impact of which on the condensation heat transfer coefficient (HTC) remains uncertain. Additionally, the connection between hazards arising from steam condensation and hydrogen combustion requires further exploration, despite the challenges faced in conducting real-time experiments. One proposed solution involves substituting hydrogen with helium in experiments to simulate localized containment behaviour
- (ii) Some studies, such as Malet et al. [147], serve as catalysts for further investigation, demonstrating the significant influence of NCG type on steam condensation. The NCG composition strongly influences the mixing properties especially the interface formation
- (iii) Previous experiments have mainly focused on studying heat transfer in condensation under saturated steam conditions. However, in assessing thermal hydraulics during severe accidents, it is crucial to consider condensation with a mix of superheated steam and NCGs. Unfortunately, the data from this perspective is scarce

- (iv) Ocean-based nuclear reactors are vital for addressing challenges like insufficient coolant and public opposition to nuclear energy. However, there is a research gap in understanding steam condensation under rolling motion, a common occurrence in ocean environments. This motion introduces centrifugal and tangential accelerations, necessitating more exploration into condensation heat transfer specific to the rolling motion experienced by oceanic nuclear reactors. Further research and development in this area are crucial
- (v) The literature highlights the need for large-scale experiments to understand natural circulation and hydrogen stratification effects on local heat transfer. Simplified models, focusing on dominant physical phenomena, are suggested for analyzing flow in large volumes, such as pressurized water reactor (PWR) containments with capacities up to $80,000 \text{ m}^3$
- (vi) In NPPs, steam condensation on containment structures can play a major role in nuclear accidents. It regulates containment pressurization, impacting safety measures like the containment cooling system. Recent advances in computational fluid dynamics (CFD) wall condensation models offer opportunities for detailed studies in mixed convection regimes during extended accident transients. There is a crucial need for model validation through diverse tests and large-scale experiments for real-world applicability, refining models, and understanding the limitations
- (vii) Investigating wall film condensation in nuclear engineering is a growing and challenging research area. Emulating condensation processes on various scales requires advanced techniques. The lack of studies on multiscale simulation using CFD and system analysis codes highlights the need for more comprehensive exploration. Increasing research efforts can enhance our understanding of wall film condensation, accelerate model development, and significantly impact the design of heat transfer systems in the nuclear industry, yielding substantial benefits
- (viii) Newly developed correlations crafted using machine learning (ML) techniques show promise and can provide accurate comparisons with experimental studies. By detecting complex patterns and correlations of CFD and experimental data, ML can prove to be an ideal tool for predicting condensation in NPPs, allowing engineers to improve design, enhance safety, optimize efficiency, manage risks, and promote sustainable and reliable nuclear energy
- f*: Degradation factor (-)
g: Gravitational acceleration (m/s^2)
h_{fg}: Latent heat of vaporization (J/kg)
h: Heat transfer coefficient ($\text{W/m}^2\cdot\text{K}$)
H: Height (m)
k: Thermal conductivity ($\text{W/m}\cdot\text{K}$)
L: Characteristic dimension (m)
M: Molecular weight (g/mole)
m''_{v,i}: Condensation mass flux ($\text{kg/m}^2\cdot\text{s}$)
P: Pressure (MPa)
R: Ideal gas constant ($\text{J/mole}\cdot\text{K}$)
*R*²: Coefficient of determination (-)
T: Temperature (K)
u, v: Velocity vector components in *x*-axis and *y*-axis, respectively (m/s)
ν_f: Kinematic viscosity (m^2/s)
w: Mass fraction (-)
Ẇ: Condensation rate
X: Mole fraction (-)
- Abbreviations*
- ANNs: Artificial neural networks
 BWR: Boiling water reactor
 CFD: Computational fluid dynamics
 CNN: Convolutional neural network
 ESBWR: Economic Simplified Boiling Water Reactor
 GBL: Gas boundary layer
 GP: Genetic programming
 HTC: Heat transfer coefficient
 HMTA: Heat and mass transfer analogy
 LBL: Liquid boundary layer
 LOCA: Loss-of-coolant accident
 LP: Lumped parameter
 MAE: Mean absolute error
 MAPE: Mean absolute percentage error
 MARD: Mean absolute relative deviation
 MGGP: Multigene genetic programming
 ML: Machine learning
 MLP: Multilayer perceptron
 MSLB: Main steam line break
 NCGs: Noncondensable gases
 NPPs: Nuclear power plants
 PCCS: Passive containment cooling system
 PWR: Pressurized water reactor
 RBFNs: Radial basis function networks
 RCS: Reactor coolant system
 RHRS: Residual heat removal system
 RMSE: Root mean square error
 SG: Steam generator
- Nondimensional Numbers*
- Gr: Grashof number = $(g\rho_b(\rho_l - \rho_b)L^3)/\mu^2, [-]$
 Nu: Nusselt number = $hl/k, [-]$
 Pr: Prandtl number = $c_p\mu/k, [-]$
 Re_{film}: Film Reynolds number = $4\dot{m}_0/\mu \cdot 2\pi r, [-]$
 Ri: Richardson number = $\text{Gr}/\text{Re}^2, [-]$
 Sc: Schmidt number = $\mu/\rho D, [-]$

Nomenclature

- c*: Molar concentration (mole/m^3)
c_p: Specific heat capacity ($\text{J/kg}\cdot\text{K}$)
D: Diffusion coefficient (m^2/s)

Sh: Sherwood number = $h_c L / k_c$, [-]
 Ma: Mach number = u / c , [-]
 Ja: Jacob number = $c_p (T_w - T_{sat}) / h_{fg}$, [-]

Subscript

a: Air
 cond: Condensation
 conv: Convection
 cr: Critical
 g: Gas/NCG-steam mixture
 grav: Gravity
 h: Hydrogen
 he: Helium
 i: Interface
 l: liquid
 NC: Natural convection
 Nu: Nusselt
 sat: Saturation condition
 ss: Shear stress
 tot: Total
 v: Vapor/steam
 w: Wall
 0: Low mass transfer or reference value

Greek Symbols

α : Thermal diffusivity (m^2/s)
 Γ : Mass flow rate per unit width ($kg/m \cdot s$)
 δ : Condensation film thickness (m)
 Θ : Suction factor (-)
 μ : Dynamic viscosity (Pa.s)
 ρ : Density (kg/m^3)
 \sum_v : Volumetric diffusion
 τ : Shear stress (N/m^2)
 C: Helium/hydrogen-to-NCG ratio

Data Availability

Data will be made available on request.

Conflicts of Interest

The authors declare that there are no conflicts of interest regarding the publication of this article.

Acknowledgments

This investigation was conducted with financial support from the project, entitled, Validation of Safety Analysis Code and Assessment of Thermal-Hydraulic Behaviours of APR1400 via OECD-ATLAS Phase 3,” Grant No. 8434000468, funded by the Federal Authority for Nuclear Regulation (FANR) in the United Arab Emirates.

References

- [1] C. Byun, D. Jerng, N. Todreas, and M. Driscoll, “Conceptual design and analysis of a semi-passive containment cooling system for a large concrete containment,” *Nuclear Engineering and Design*, vol. 199, no. 3, pp. 227–242, 2000.
- [2] T. L. Schulz, “Westinghouse AP1000 advanced passive plant,” *Nuclear Engineering and Design*, vol. 236, no. 14–16, pp. 1547–1557, 2006.
- [3] J. C. de la Rosa, A. Escrivá, L. E. Herranz, T. Cicero, and J. L. Muñoz-Cobo, “Review on condensation on the containment structures,” *Progress in Nuclear Energy*, vol. 51, no. 1, pp. 32–66, 2009.
- [4] D. F. Othmer, “The condensation of steam,” *Industrial & Engineering Chemistry*, vol. 21, no. 6, pp. 576–583, 1929.
- [5] S. J. Meisenburg, R. M. Boarts, and W. L. Badger, *The Influence of Small Concentrations of Air in Steam on the Steam-Film Coefficient of Heat Transfer*, University of Michigan, 1935.
- [6] H. Uchida, A. Oyama, and Y. Togo, *Evaluation of Post-Incident Cooling Systems of Light Water Power Reactors*, Tokyo Univ, 1964.
- [7] H. Al-Diwany and J. Rose, “Free convection film condensation of steam in the presence of non-condensing gases,” *International Journal of Heat and Mass Transfer*, vol. 16, no. 7, pp. 1359–1369, 1973.
- [8] D. G. Kroger and W. M. Rohsenow, “Condensation heat transfer in the presence of a non-condensable gas,” *International Journal of Heat and Mass Transfer*, vol. 11, no. 1, pp. 15–26, 1968.
- [9] M. K. Yadav, S. Khandekar, and P. K. Sharma, “An integrated approach to steam condensation studies inside reactor containments: a review,” *Nuclear Engineering and Design*, vol. 300, pp. 181–209, 2016.
- [10] A. S. Dalkilic and S. Wongwises, “Intensive literature review of condensation inside smooth and enhanced tubes,” *International Journal of Heat and Mass Transfer*, vol. 52, no. 15–16, pp. 3409–3426, 2009.
- [11] A. A. Ganguli, S. K. Dahikar, M. S. Gandhi, J. B. Joshi, and P. K. Vijayan, “Heat transfer and flow pattern in co-current downward steam condensation in vertical pipes-II: comparison with published works,” *The Canadian Journal of Chemical Engineering*, vol. 91, no. 5, pp. 974–991, 2013.
- [12] J. Huang, J. Zhang, and L. Wang, “Review of vapor condensation heat and mass transfer in the presence of non-condensable gas,” *Applied Thermal Engineering*, vol. 89, pp. 469–484, 2015.
- [13] W. Chen, K. Hui, B. Wang, Q. Zhao, D. Chong, and J. Yan, “Review of the tube external condensation heat transfer characteristic of the passive containment cooling system in nuclear power plant,” *Annals of Nuclear Energy*, vol. 157, p. 108226, 2021.
- [14] P. K. Bhowmik, J. P. Schlegel, and S. Revankar, “State-of-the-art and review of condensation heat transfer for small modular reactor passive safety: experimental studies,” *International Journal of Heat and Mass Transfer*, vol. 192, p. 122936, 2022.
- [15] J. Su, L. Fan, and L. Gao, “Review of steam condensation heat transfer under containment cooling system condition,” *Atomic Energy Science and Technology*, vol. 50, no. 11, p. 1956, 2016.
- [16] J. Green and K. Almenasb, “An overview of the primary parameters and methods for determining condensation,” *Nuclear Safety*, vol. 37, no. 1, p. 26, 1996.
- [17] F. Liu, Z. Sun, M. Ding, and H. Bian, “Research progress of hydrogen behaviors in nuclear power plant containment under severe accident conditions,” *International Journal of Hydrogen Energy*, vol. 46, no. 73, pp. 36477–36502, 2021.

- [18] R. Parin, *Experimental and Theoretical Analysis of Condensation over Nanoengineered Surfaces*, Universita' Degli Studi Di Padova, 2015.
- [19] J. Rose, "Dropwise condensation theory and experiment: a review," *Proceedings of the Institution of Mechanical Engineers, Part A: Journal of Power and Energy*, vol. 216, no. 2, pp. 115–128, 2002.
- [20] C. A. Miller and P. Neogi, *Interfacial phenomena: equilibrium and dynamic effects*, vol. 139, CRC Press, 2007.
- [21] K. Vierow, "Enhancement of nuclear power plant safety by condensation-driven passive heat removal systems," *Thermal Engineering in Power Systems*, vol. 1, pp. 141–170, 2008.
- [22] G. F. Hewitt, G. L. Shires, and T. Bott, *Process Heat Transfer*, Begell House, 1994.
- [23] B. K. Purohit, Z. Hussain, and P. S. Prasad, "Boiling and condensation, in heat transfer," in *Heat transfer-fundamentals, enhancement and applications* IntechOpen.
- [24] I. Tanasawa, "Advances in condensation heat transfer," in *Advances in Heat Transfer*, vol. 21, J. P. Hartnett, T. F. Irvine, and Y. I. Cho, Eds., pp. 55–139, Elsevier, 1991.
- [25] R. W. Serth, "11- Condensers," in *Process Heat Transfer*, R. W. Serth, Ed., pp. 539–628, Academic Press, Oxford, 2007.
- [26] J. Van der Walt and D. G. Kroger, *Heat transfer resistances during film condensation*, International Heat Transfer Conference Digital Library, Begell House Inc., 1974.
- [27] H. D. Baehr and K. Stephan, *Wärme-und stoffübertragung*, vol. 7, Springer, 1994.
- [28] C. A. Depew and R. L. Reisbig, "Vapor condensation on a horizontal tube using Teflon to promote dropwise condensation," *Industrial & Engineering Chemistry Process Design and Development*, vol. 3, no. 4, pp. 365–369, 1964.
- [29] J. Rose, "Laminar film condensation of pure vapors," in *Handbook of Phase Change: Boiling and Condensation*, pp. 523–536, Taylor & Francis Philadelphia, 1999.
- [30] D. Labuntsov, "Heat transfer in film condensation of pure steam on vertical surfaces and horizontal tubes," *Teplotenergetika*, vol. 3, pp. 3–12, 1960.
- [31] D. Butterworth, *Introduction to heat transfer*, vol. 18, Oxford University Press for the Design Council, the British Standards Institution and the Council of Engineering Institutions, 1977.
- [32] W. Nusselt, "Die oberflächenkondensation des wasserdampfes," *VDI-Zs*, vol. 60, p. 541, 1916.
- [33] E. M. Sparrow and J. L. Gregg, "A boundary-layer treatment of laminar-film condensation," *Journal of Heat Transfer*, vol. 81, no. 1, pp. 13–18, 1959.
- [34] E. M. Sparrow and J. L. Gregg, "Laminar condensation heat transfer on a horizontal cylinder," *Journal of Heat Transfer*, vol. 81, no. 4, pp. 291–295, 1959.
- [35] A. E. Dukler, "Fluid mechanics and heat transfer in vertical falling film systems," *Chemical Engineering Progress Symposium Series*, vol. 56, 1960.
- [36] I. G. Shekrladze and V. Gomelaury, "Theoretical study of laminar film condensation of flowing vapour," *International Journal of Heat and Mass Transfer*, vol. 9, no. 6, pp. 581–591, 1966.
- [37] A. Cavallini, G. Censi, D. Del Col et al., "Condensation inside and outside smooth and enhanced tubes—a review of recent research," *International Journal of Refrigeration*, vol. 26, no. 4, pp. 373–392, 2003.
- [38] R. Kumar, H. Varma, B. Mohanty, and K. Agrawal, "Augmentation of heat transfer during filmwise condensation of steam and R-134a over single horizontal finned tubes," *International Journal of Heat and Mass Transfer*, vol. 45, no. 1, pp. 201–211, 2002.
- [39] S. Memory, V. Adams, and P. Marto, "Free and forced convection laminar film condensation on horizontal elliptical tubes," *International Journal of Heat and Mass Transfer*, vol. 40, no. 14, pp. 3395–3406, 1997.
- [40] H. Merte Jr., "Condensation heat transfer," in *Advances in heat transfer*, vol. 9, pp. 181–272, Elsevier, 1973.
- [41] W. J. Minkowycz, *Laminar Film Condensation of Water Vapor on an Isothermal Vertical Surface*, University of Minnesota, 1965.
- [42] W. Minkowycz and E. Sparrow, "Condensation heat transfer in the presence of noncondensables, interfacial resistance, superheating, variable properties, and diffusion," *International Journal of Heat and Mass Transfer*, vol. 9, no. 10, pp. 1125–1144, 1966.
- [43] E. Sparrow, W. Minkowycz, and M. Saddy, "Forced convection condensation in the presence of noncondensables and interfacial resistance," *International Journal of Heat and Mass Transfer*, vol. 10, no. 12, pp. 1829–1845, 1967.
- [44] K. Stephan, *Heat transfer in condensation and boiling*, Springer, Berlin, Heidelberg, 1992.
- [45] V. P. Carey, *Liquid-Vapor Phase-Change Phenomena: An Introduction to the Thermophysics of Vaporization and Condensation Processes in Heat Transfer Equipment*, CRC Press, 2020.
- [46] M. L. Corradini, "Turbulent condensation on a cold wall in the presence of a noncondensable gas," *Nuclear Technology*, vol. 64, no. 2, pp. 186–195, 1984.
- [47] M. Bucci, *Experimental and Computational Analysis of Condensation Phenomena for the Thermal-Hydraulic Analysis of LWRs Containments*, [Ph.D. thesis], University of Pisa, 2009.
- [48] C. Wilke and C. Lee, "Estimation of diffusion coefficients for gases and vapors," *Industrial & Engineering Chemistry*, vol. 47, no. 6, pp. 1253–1257, 1955.
- [49] J. Martin-Valdepenas, M. Jimenez, F. Martin-Fuertes, and J. F. Benitez, "Comparison of film condensation models in presence of non-condensable gases implemented in a CFD code," *Heat and Mass Transfer*, vol. 41, no. 11, pp. 961–976, 2005.
- [50] B. E. Poling, *The Properties of Gases and Liquids*, McGRAW-HILL, 2004.
- [51] S. Benteboula and F. Dabbene, "Modeling of wall condensation in the presence of noncondensable light gas," *International Journal of Heat and Mass Transfer*, vol. 151, p. 119313, 2020.
- [52] K. M. Vierow, *Behavior of Steam-Air Systems Condensing in Cocurrent Vertical Downflow*, [M.S. thesis], Univ. of California, Berkeley, 1990.
- [53] H. Terasaka and A. Makita, "Numerical analysis of the PHEBUS containment thermal hydraulics," *Journal of Nuclear Science and Technology*, vol. 34, no. 7, pp. 666–678, 1997.
- [54] K. Asano, Y. Nakano, and M. Inaba, "Forced convection film condensation of vapors in the presence of noncondensable gas on a small vertical flat plate," *Journal of Chemical Engineering of Japan*, vol. 12, no. 3, pp. 196–202, 1979.
- [55] I. Phebus, *FPT0 final report*, IPSN/DRS/SEA/LERES/97/1815 CLT. 47 12 40, Cadarache, Francia, 1997.
- [56] M. H. Kim and M. Corradini, "Modeling of condensation heat transfer in a reactor containment," *Nuclear Engineering and Design*, vol. 118, no. 2, pp. 193–212, 1990.

- [57] K. M. Vierow and V. E. Schrock, *Condensation in a Natural Circulation Loop with Noncondensable Gases, 1*, Japan Society of Multiphase Flow, Japan, 1991, http://inis.iaea.org/search/search.aspx?orig_q=RN:24054054.
- [58] S. Z. Kuhn, V. E. Schrock, and P. F. Peterson, "An investigation of condensation from steam-gas mixtures flowing downward inside a vertical tube," *Nuclear Engineering and Design*, vol. 177, no. 1-3, pp. 53-69, 1997.
- [59] K.-Y. Lee and M. H. Kim, "Experimental and empirical study of steam condensation heat transfer with a noncondensable gas in a small-diameter vertical tube," *Nuclear Engineering and Design*, vol. 238, no. 1, pp. 207-216, 2008.
- [60] A. P. Colburn and O. A. Hougen, "Design of cooler condensers for mixtures of vapors with noncondensing gases," *Industrial & Engineering Chemistry*, vol. 26, no. 11, pp. 1178-1182, 1934.
- [61] T. H. Chilton and A. P. Colburn, "Mass transfer (absorption) coefficients prediction from data on heat transfer and fluid friction," *Industrial & Engineering Chemistry*, vol. 26, no. 11, pp. 1183-1187, 1934.
- [62] R. B. Bird, "Transport phenomena," *Applied Mechanics Reviews*, vol. 55, no. 1, pp. R1-R4, 2002.
- [63] D. Spalding, "A standard formulation of the steady convective mass transfer problem," *International Journal of Heat and Mass Transfer*, vol. 1, no. 2-3, pp. 192-207, 1960.
- [64] J. H. Lienhard, *A Heat Transfer Textbook*, Phlogistron, 2005.
- [65] Y. Liao and K. Vierow, "A generalized diffusion layer model for condensation of vapor with noncondensable gases," *Journal of Heat Transfer*, vol. 129, no. 8, pp. 988-994, 2007.
- [66] W. Ambrosini, N. Forgone, A. Manfredini, and F. Oriolo, "On various forms of the heat and mass transfer analogy: discussion and application to condensation experiments," *Nuclear Engineering and Design*, vol. 236, no. 9, pp. 1013-1027, 2006.
- [67] A. Dehbi, "A generalized correlation for steam condensation rates in the presence of air under turbulent free convection," *International Journal of Heat and Mass Transfer*, vol. 86, pp. 1-15, 2015.
- [68] D. Tecdoc, *Considerations on the application of the iaea safety requirements for design of nuclear power plants*, International Atomic Energy Agency, 2014.
- [69] P. F. Peterson, V. E. Schrock, and T. Kageyama, "Diffusion layer theory for turbulent vapor condensation with noncondensable gases," *Journal of Heat Transfer*, vol. 115, no. 4, pp. 998-1003, 1993.
- [70] I. Tkatschenko, E. Studer, and H. Paillère, *MISTRA facility for containment lumped parameter and CFD codes validation. Example of the International Standard Problem ISP47*, Nuclear Energy for New Europe, 2005.
- [71] M. H. Anderson, *Steam Condensation on Cold Walls of Advanced PWR Containments*, The University of Wisconsin-Madison, 1998.
- [72] L. E. Herranz, M. H. Anderson, and M. L. Corradini, "A diffusion layer model for steam condensation within the AP600 containment," *Nuclear Engineering and Design*, vol. 183, no. 1-2, pp. 133-150, 1998.
- [73] J. G. Collier and J. R. Thome, *Convective Boiling and Condensation*, Clarendon Press, 1994.
- [74] J. Lee, G.-C. Park, and H. K. Cho, "Improvement of CUPID code for simulating filmwise steam condensation in the presence of noncondensable gases," *Nuclear Engineering and Technology*, vol. 47, no. 5, pp. 567-578, 2015.
- [75] A. Dehbi, "On the adequacy of wall functions to predict condensation rates from steam-noncondensable gas mixtures," *Nuclear Engineering and Design*, vol. 265, pp. 25-34, 2013.
- [76] E. F. Tanjung, S. A. Albdour, Y. U. Jeong, and D. Jo, "Critical heat flux (CHF) in pool boiling under static and rolling conditions," *Nuclear Engineering and Technology*, vol. 52, no. 3, pp. 520-529, 2020.
- [77] S. A. Albdour, E. F. Tanjung, and D. Jo, "Experimental study of critical heat flux mechanism on a vertical heated surface under rolling motion," *Annals of Nuclear Energy*, vol. 151, p. 107967, 2021.
- [78] A. Sun, J. Cheng, C. Yan, D. Zhu, C. Tian, and P. Li, "Experimental study on condensation heat transfer characteristics in C-shaped tube under rolling conditions," *Nuclear Engineering and Design*, vol. 408, article 112327, 2023.
- [79] N. Aksan, J. H. Choi, Y. J. Chung et al., *Passive safety systems and natural circulation in water cooled nuclear power plants*, International Atomic Energy Agency, 2009.
- [80] S. Tower, T. Schulz, and R. Vijuk, "Passive and simplified system features for the advanced Westinghouse 600 MWe PWR," *Nuclear Engineering and Design*, vol. 109, no. 1-2, pp. 147-154, 1988.
- [81] S. W. Lee, S. Heo, H. U. Ha, and H. G. Kim, "The concept of the innovative power reactor," *Nuclear Engineering and Technology*, vol. 49, no. 7, pp. 1431-1441, 2017.
- [82] W. Zhou, B. Wolf, and S. Revankar, "Assessment of RELAP5/MOD3. 3 condensation models for the tube bundle condensation in the PCCS of ESBWR," *Nuclear Engineering and Design*, vol. 264, pp. 111-118, 2013.
- [83] J. Xing, D. Song, and Y. Wu, "HPR1000: advanced pressurized water reactor with active and passive safety," *Engineering*, vol. 2, no. 1, pp. 79-87, 2016.
- [84] H. Ha, S. Lee, and H. Kim, "Optimal design of passive containment cooling system for innovative PWR," *Nuclear Engineering and Technology*, vol. 49, no. 5, pp. 941-952, 2017.
- [85] J. Rose, "Condensation of a vapour in the presence of a non-condensing gas," *International Journal of Heat and Mass Transfer*, vol. 12, no. 2, pp. 233-237, 1969.
- [86] J. Rose, "Approximate equations for forced-convection condensation in the presence of a non-condensing gas on a flat plate and horizontal tube," *International Journal of Heat and Mass Transfer*, vol. 23, no. 4, pp. 539-546, 1980.
- [87] C. Lee, T. Liu, Y. Way, and D. Hsia, "Investigation of mid-loop operation with loss of RHR at INER integral system test (IIST) facility," *Nuclear Engineering and Design*, vol. 163, no. 3, pp. 349-358, 1996.
- [88] Y.-S. Kim, H.-S. Park, S. Cho, K.-Y. Choi, and K.-H. Kang, "Reflux condensation behavior in SBLOCA tests of ATLAS facility," *Annals of Nuclear Energy*, vol. 99, pp. 227-239, 2017.
- [89] K. Almenas, "Heat transfer from saturated and superheated atmospheres for containment analysis," *Nuclear Engineering and Design*, vol. 71, no. 1, pp. 1-14, 1982.
- [90] J. J. Carbajo, "Heat transfer coefficients under LOCA conditions in containment buildings," *Nuclear Engineering and Design*, vol. 65, no. 3, pp. 369-386, 1981.
- [91] D. Paladino, G. Mignot, R. Kapulla et al., "OECD/NEA HYMERES project: for the analysis and mitigation of a severe accident leading to hydrogen release into a nuclear plant containment," *Proceedings of ICAPP*, vol. 2014, pp. 6-9, 2014.

- [92] H. Bian, Z. Sun, M. Ding, and N. Zhang, "Local phenomena analysis of steam condensation in the presence of air," *Progress in Nuclear Energy*, vol. 101, pp. 188–198, 2017.
- [93] P. F. Peterson, "Diffusion layer modeling for condensation with multicomponent noncondensable gases," *Journal of Heat Transfer*, vol. 122, no. 4, pp. 716–720, 2000.
- [94] X. Ma, J. Ma, H. Tong, and H. Jia, "The investigation on heat transfer characteristics of steam condensation in presence of noncondensable gas under natural convection," *Science and Technology of Nuclear Installations*, vol. 2021, Article ID 6689597, 13 pages, 2021.
- [95] M. A. Amidu, S. A. Olatubosun, A. Ayodeji, and Y. Addad, "Severe accident in high-power light water reactors: mitigating strategies, assessment methods and research opportunities," *Progress in Nuclear Energy*, vol. 143, p. 104062, 2022.
- [96] M. A. Amidu and Y. Addad, "The influence of the water ingress and melt eruption model on the MELCOR code prediction of molten corium-concrete interaction in the APR-1400 reactor cavity," *Nuclear Engineering and Technology*, vol. 54, no. 4, pp. 1508–1515, 2022.
- [97] J. Martín-Valdepeñas, M. Jiménez, F. Martín-Fuertes, and J. Fernández, "Improvements in a CFD code for analysis of hydrogen behaviour within containments," *Nuclear Engineering and Design*, vol. 237, no. 6, pp. 627–647, 2007.
- [98] H. Liu, N. E. Todreas, and M. J. Driscoll, "An experimental investigation of a passive cooling unit for nuclear plant containment," *Nuclear Engineering and Design*, vol. 199, no. 3, pp. 243–255, 2000.
- [99] A. A. Dehbi, *The effects of noncondensable gases on steam condensation under turbulent natural convection conditions*, Diss. Massachusetts Institute of Technology, 1991.
- [100] X. Ma, X. Xiao, H. Jia et al., "Experimental research on steam condensation in presence of non-condensable gas under high pressure," *Annals of Nuclear Energy*, vol. 158, p. 108282, 2021.
- [101] X. Cheng, P. Bazin, P. Cornet et al., "Experimental data base for containment thermohydraulic analysis," *Nuclear Engineering and Design*, vol. 204, no. 1-3, pp. 267–284, 2001.
- [102] S. Kudriakov, F. Dabbene, E. Studer et al., "The TONUS CFD code for hydrogen risk analysis: physical models, numerical schemes and validation matrix," *Nuclear Engineering and Design*, vol. 238, no. 3, pp. 551–565, 2008.
- [103] T. F. Kanzleiter, K. O. Fischer, H. J. Allelein, and S. Schwarz, *Thai multi-compartment containment experiments with atmosphere stratification*, Nureth 11, eleventh international topical meeting on nuclear reactor thermal hydraulics, France, 2005, http://inis.iaea.org/search/search.aspx?orig_q=RN:37062738.
- [104] J. Xiao and J. R. Travis, "How critical is turbulence modeling in gas distribution simulations of large-scale complex nuclear reactor containment?," *Annals of Nuclear Energy*, vol. 56, pp. 227–242, 2013.
- [105] T. Tagami, *Interim Report on Safety Assessments and Facilities Establishment Project for June 1965, No. 1*, Japanese Atomic Energy Research Agency, 1965.
- [106] J. Su, Z. Sun, M. Ding, and G. Fan, "Analysis of experiments for the effect of noncondensable gases on steam condensation over a vertical tube external surface under low wall subcooling," *Nuclear Engineering and Design*, vol. 278, pp. 644–650, 2014.
- [107] J. Su, Z. Sun, G. Fan, and M. Ding, "Experimental study of the effect of non-condensable gases on steam condensation over a vertical tube external surface," *Nuclear Engineering and Design*, vol. 262, pp. 201–208, 2013.
- [108] U.-J. Lee and G.-C. Park, "Experimental study on hydrogen behavior at a subcompartment in the containment building," *Nuclear Engineering and Design*, vol. 217, no. 1-2, pp. 41–47, 2002.
- [109] G. Fan, P. Tong, Z. Sun, and Y. Chen, "Development of a new empirical correlation for steam condensation rates in the presence of air outside vertical smooth tube," *Annals of Nuclear Energy*, vol. 113, pp. 139–146, 2018.
- [110] Y. Kataoka, T. Fukui, S. Hatamiya, T. Nakao, M. Naitoh, and I. Sumida, "Experiments on convection heat transfer along a vertical flat plate between pools with different temperatures," *Nuclear Technology*, vol. 99, no. 3, pp. 386–396, 1992.
- [111] M. Murase, Y. Kataoka, and T. Fujii, "Evaporation and condensation heat transfer with a noncondensable gas present," *Nuclear Engineering and Design*, vol. 141, no. 1–2, pp. 135–143, 1993.
- [112] H.-K. Ahn, Y.-G. Lee, J.-W. Kim, and G.-C. Park, "Experimental study on the condensation heat transfer with non-condensable gas at high pressure," *Proceedings of Korean Nuclear Spring Meeting*, vol. 38, 2007.
- [113] B. Cao, Y. Li, Y. Lu, S. Zhou, H. Bian, and M. Ding, "Experimental study of air–steam condensation on the influence of tube diameter and inclination angle," *Nuclear Engineering and Design*, vol. 381, p. 111357, 2021.
- [114] M. Kawakubo, M. Aritomi, H. Kikura, and T. Komeno, "An experimental study on the cooling characteristics of passive containment cooling systems," *Journal of Nuclear Science and Technology*, vol. 46, no. 4, pp. 339–345, 2009.
- [115] K. Zhang, J. Hu, Z. Nan, Z. Chen, and N. Wang, "Experimental study of heat transfer characteristics on condensation in the presence of NCG through thermal resistance analysis," *Progress in Nuclear Energy*, vol. 131, article 103591, 2021.
- [116] Y.-G. Lee, Y.-J. Jang, and D.-J. Choi, "An experimental study of air–steam condensation on the exterior surface of a vertical tube under natural convection conditions," *International Journal of Heat and Mass Transfer*, vol. 104, pp. 1034–1047, 2017.
- [117] L. Wang, P. Chen, Y. Zhou et al., "Experimental study on the condensation of steam with air out of the vertical tube bundles," *Frontiers in Energy Research*, vol. 6, p. 32, 2018.
- [118] J. Kang, H. Kim, J. Bak, S.-G. Lim, and B. Yun, "Condensation of steam mixed with non-condensable gas on vertical heat exchanger tubes in circumstances with free convection," *International Journal of Heat and Mass Transfer*, vol. 169, article 120925, 2021.
- [119] Y.-J. Jang, D.-J. Choi, Y.-G. Lee, and S. Kim, "Experimental study of condensation heat transfer in the presence of non-condensable gas on the vertical tube," in *Proceedings of the 16th International Topical Meeting on Nuclear Reactor Thermal Hydraulics*, pp. 6096–6109, Chicago, IL, 2015.
- [120] U.-K. Kim, J.-W. Yoo, Y.-J. Jang, and Y.-G. Lee, "Measurement of heat transfer coefficients for steam condensation on a vertical 21.5-mm-O.D. tube in the presence of air," *Journal of Nuclear Science and Technology*, vol. 57, no. 8, pp. 905–916, 2020.
- [121] B.-U. Bae, S. Kim, Y.-S. Park, and K.-H. Kang, "Experimental investigation on condensation heat transfer for bundle tube heat exchanger of the PCCS (passive containment cooling system)," *Annals of Nuclear Energy*, vol. 139, p. 107285, 2020.

- [122] A. Dehbi, "A unified correlation for steam condensation rates in the presence of air-helium mixtures under naturally driven flows," *Nuclear Engineering and Design*, vol. 300, pp. 601–609, 2016.
- [123] A. Dehbi, "Correcting for tube curvature effects on condensation in the presence of a noncondensable gas in laminar regimes," *International Journal of Heat and Mass Transfer*, vol. 151, p. 119384, 2020.
- [124] S.-Z. Kuhn, *Investigation of heat transfer from condensing steam-gas mixtures and turbulent films flowing downward inside a vertical tube*, University of California, Berkeley, 1995.
- [125] F. Ağlar and A. Tanrikut, "A new heat transfer correlation for condensation in the presence of air and its implementation into RELAP5/MOD3. 3," *Nuclear Technology*, vol. 161, no. 3, pp. 286–298, 2008.
- [126] H. S. Park and H. C. No, "A condensation experiment in the presence of noncondensables in a vertical tube of a passive containment cooling system and its assessment with RELAP5/MOD3. 2," *Nuclear Technology*, vol. 127, no. 2, pp. 160–169, 1999.
- [127] M. Siddique, *The effects of noncondensable gases on steam condensation under forced convection conditions*, Massachusetts Institute of Technology, Dept. of Nuclear Engineering, 1992.
- [128] H. Akaki, Y. Kataoka, and M. Murase, "Measurement of condensation heat transfer coefficient inside a vertical tube in the presence of noncondensable gas," *Journal of Nuclear Science and Technology*, vol. 32, no. 6, pp. 517–526, 1995.
- [129] H. A. Hasanein, M. S. Kazimi, and M. W. Golay, "Forced convection in-tube steam condensation in the presence of non-condensable gases," *International Journal of Heat and Mass Transfer*, vol. 39, no. 13, pp. 2625–2639, 1996.
- [130] N. K. Maheshwari, *Studies on Passive Containment Cooling System of Indian Advanced Heavy Water Reactor*, Tokyo Institute of Technology, 2006.
- [131] M. Murase and Y. Utanohara, "Numerical simulation of wall condensation from a superheated steam and air mixture in a vertical pipe," *Nuclear Technology*, vol. 209, no. 7, pp. 1086–1100, 2023.
- [132] M. Murase, Y. Utanohara, R. Goda, T. Shimamura, S. Hosokawa, and A. Tomiyama, "Measurements of temperature distributions and condensation heat fluxes for downward flows of steam-air mixture in a circular pipe," *Japanese Journal of Multiphase Flow*, vol. 33, no. 4, pp. 405–416, 2019.
- [133] B. Chatterjee, D. Mukhopadhyay, H. G. Lele et al., "Analyses for VVER-1000/320 reactor for spectrum of break sizes along with SBO," *Annals of Nuclear Energy*, vol. 37, no. 3, pp. 359–370, 2010.
- [134] J. Birchley, T. J. Haste, and M. Richner, "Accident management following loss of residual heat removal during mid-loop operation in a Westinghouse two-loop PWR," *Nuclear Engineering and Design*, vol. 238, no. 9, pp. 2173–2181, 2008.
- [135] Q. Nguyen and S. Banerjee, *Analysis of experimental data on condensation in an inverted U-tube. Final report*, California Univ., Santa Barbara (USA). Dept. of Chemical and Nuclear Engineering, 1985.
- [136] S. B. Al-Shammari, D. R. Webb, and P. Heggs, "Condensation of steam with and without the presence of non-condensable gases in a vertical tube," *Desalination*, vol. 169, no. 2, pp. 151–160, 2004.
- [137] Y. Liao, S. Guentay, D. Suckow, and A. Dehbi, "Reflux condensation of flowing vapor and non-condensable gases counter-current to laminar liquid film in a vertical tube," *Nuclear Engineering and Design*, vol. 239, no. 11, pp. 2409–2416, 2009.
- [138] Y. Pan, "Condensation characteristics inside a vertical tube considering the presence of mass transfer, vapor velocity and interfacial shear," *International Journal of Heat and Mass Transfer*, vol. 44, no. 23, pp. 4475–4482, 2001.
- [139] S. Thumm, C. Philipp, and U. Gross, "Film condensation of water in a vertical tube with countercurrent vapour flow," *International Journal of Heat and Mass Transfer*, vol. 44, no. 22, pp. 4245–4256, 2001.
- [140] U. Gross and C. Philipp, "Conjugated shear stress and Prandtl number effects on reflux condensation heat transfer inside a vertical tube," *International Journal of Heat and Mass Transfer*, vol. 49, no. 1-2, pp. 144–153, 2006.
- [141] U. Gross, T. Storch, C. Philipp, and A. Doeg, "Wave frequency of falling liquid films and the effect on reflux condensation in vertical tubes," *International Journal of Multiphase Flow*, vol. 35, no. 4, pp. 398–409, 2009.
- [142] K.-W. Lee, H. C. No, I.-C. Chu, Y. M. Moon, and M.-H. Chun, "Local heat transfer during reflux condensation mode in a U-tube with and without noncondensable gases," *International Journal of Heat and Mass Transfer*, vol. 49, no. 11–12, pp. 1813–1819, 2006.
- [143] Y. Moon, H. Park, and Y. Bang, *Assessment of RELAP5/MOD3. 2 for reflux condensation experiment*, Citeseer, 2000.
- [144] K. Vierow, T. Wu, and T. Nagae, *Experimental investigation of reflux condensation heat transfer in PWR steam generator tubes in the presence of noncondensable gases*, NURETH-10, Seoul (Korea, Republic of), 2003.
- [145] F. Hassaninejadfarahani, *Numerical Analysis of Reflux Condensation*, University of Manitoba, Winnipeg, Manitoba, Canada, 2016.
- [146] F. Janasz, *Effect of non-condensable gases on reflux condensation in nuclear steam generator tubes*, ETH ZURICH, 2019.
- [147] J. Malet, E. Porcheron, and J. Vendel, "OECD international standard problem ISP-47 on containment thermal-hydraulics—conclusions of the TOSQAN part," *Nuclear Engineering and Design*, vol. 240, no. 10, pp. 3209–3220, 2010.
- [148] N. Oecd, *SETH-2 project panda and mistra experiments final summary report: investigation of key issues for the simulation of thermal-hydraulic conditions in water reactor containment*, NEA/CSNI, 2012.
- [149] M. K. Yadav, *Steam Condensation Studies towards Understanding Post-Severe Nuclear Accident Scenarios*, Indian Institute of Technology Kanpur Kanpur, India, 2018.
- [150] P. Sathiah, E. Komen, and D. Roekaerts, "The role of CFD combustion modeling in hydrogen safety management—part I: validation based on small scale experiments," *Nuclear Engineering and Design*, vol. 248, pp. 93–107, 2012.
- [151] International Atomic Energy Agency, *Mitigation of Hydrogen Hazards in Severe Accidents in Nuclear Power Plants*, IAEA, 2011.
- [152] I. Kljenak, M. Babić, B. Mavko, and I. Bajsić, "Modeling of containment atmosphere mixing and stratification experiment using a CFD approach," *Nuclear Engineering and Design*, vol. 236, no. 14–16, pp. 1682–1692, 2006.
- [153] P. K. Sharma, B. Gera, R. Singh, and K. Vaze, "Computational fluid dynamics modeling of steam condensation on nuclear containment wall surfaces based on semiempirical generalized

- correlations,” *Science and Technology of Nuclear Installations*, vol. 2012, Article ID 106759, 7 pages, 2012.
- [154] M. Punetha, M. K. Yadav, S. Khandekar, P. K. Sharma, and S. Ganju, “Intrinsic transport and combustion issues of steam-air-hydrogen mixtures in nuclear containments,” *International Journal of Hydrogen Energy*, vol. 45, no. 4, pp. 3340–3371, 2020.
- [155] M. Houkema, N. B. Siccama, J. A. L. à Nijeholt, and E. M. J. Komen, “Validation of the CFX4 CFD code for containment thermal-hydraulics,” *Nuclear Engineering and Design*, vol. 238, no. 3, pp. 590–599, 2008.
- [156] A. Dehbi, F. Janasz, and B. Bell, “Prediction of steam condensation in the presence of noncondensable gases using a CFD-based approach,” *Nuclear Engineering and Design*, vol. 258, pp. 199–210, 2013.
- [157] M. Punetha and S. Khandekar, “A CFD based modelling approach for predicting steam condensation in the presence of non-condensable gases,” *Nuclear Engineering and Design*, vol. 324, pp. 280–296, 2017.
- [158] J. T. Kim, R. J. Park, and G. H. Kim, “Methodology for evaluation of hydrogen safety in a NPP containment,” in *Proceedings of the KNS 2018 Spring Meeting*, Korea, Republic of: KNS, 2018 http://inis.iaea.org/search/search.aspx?orig_q=RN:50059520.
- [159] S. Kelm, M. Kampili, X. Liu et al., “The tailored CFD package ‘containmentFOAM’ for analysis of containment atmosphere mixing, H₂/CO mitigation and aerosol transport,” *Fluids*, vol. 6, no. 3, p. 100, 2021.
- [160] S. Mimouni, J.-S. Lamy, J. Lavieville, S. Guieu, and M. Martin, “Modelling of sprays in containment applications with a CMFD code,” *Nuclear Engineering and Design*, vol. 240, no. 9, pp. 2260–2270, 2010.
- [161] G. Zschaek, T. Frank, and A. D. Burns, “CFD modelling and validation of wall condensation in the presence of non-condensable gases,” *Nuclear Engineering and Design*, vol. 279, pp. 137–146, 2014.
- [162] W. Ambrosini, M. Bucci, N. Forgone et al., “Comparison and analysis of the condensation benchmark results,” in *3rd European Review Meeting on Severe Accident Research (ERMSAR-2008)*, Nesseber, Bulgaria, 2008.
- [163] G. V. Kumar, L. M. Cammiadi, S. Kelm et al., “Implementation of a CFD model for wall condensation in the presence of non-condensable gas mixtures,” *Applied Thermal Engineering*, vol. 187, article 116546, 2021.
- [164] J.-D. Li, “CFD simulation of water vapour condensation in the presence of non-condensable gas in vertical cylindrical condensers,” *International Journal of Heat and Mass Transfer*, vol. 57, no. 2, pp. 708–721, 2013.
- [165] C. W. Lee, J.-S. Yoo, and H. K. Cho, “Multi-scale simulation of wall film condensation in the presence of non-condensable gases using heat structure-coupled CFD and system analysis codes,” *Nuclear Engineering and Technology*, vol. 53, no. 8, pp. 2488–2498, 2021.
- [166] H. Y. Yoon, K. D. Kim, J. W. Kim et al., *CUPID Code Manual Volume I: Mathematical Models and Solution Methods*, Korea Atomic Energy Research Institute, 2011.
- [167] B. D. Chung, K. D. Kim, S. W. Bae et al., *MARS Code Manual Volume I: Code Structure, System Models, and Solution Methods*, Korea Atomic Energy Research Institute, 2010.
- [168] J. R. Lee and H. Y. Yoon, “Preliminary study for a PWR steam generator with CUPID/MARS multi-scale thermal-hydraulics simulation,” *Applied Thermal Engineering*, vol. 115, pp. 1245–1254, 2017.
- [169] H. K. Cho, Y. J. Cho, and H. Y. Yoon, “Heat structure coupling of CUPID and MARS for the multi-scale simulation of the passive auxiliary feedwater system,” *Nuclear Engineering and Design*, vol. 273, pp. 459–468, 2014.
- [170] A. Ayodeji, M. A. Amidu, S. A. Olatubosun, Y. Addad, and H. Ahmed, “Deep learning for safety assessment of nuclear power reactors: reliability, explainability, and research opportunities,” *Progress in Nuclear Energy*, vol. 151, article 104339, 2022.
- [171] L. Zhou, D. Garg, Y. Qiu, S.-M. Kim, I. Mudawar, and C. R. Kharangate, “Machine learning algorithms to predict flow condensation heat transfer coefficient in mini/micro-channel utilizing universal data,” *International Journal of Heat and Mass Transfer*, vol. 162, article 120351, 2020.
- [172] G. Zhu, T. Wen, and D. Zhang, “Machine learning based approach for the prediction of flow boiling/condensation heat transfer performance in mini channels with serrated fins,” *International Journal of Heat and Mass Transfer*, vol. 166, article 120783, 2021.
- [173] M. Balcilar, A. S. Dalkilic, and S. Wongwises, “Artificial neural network techniques for the determination of condensation heat transfer characteristics during downward annular flow of R134a inside a vertical smooth tube,” *International Communications in Heat and Mass Transfer*, vol. 38, no. 1, pp. 75–84, 2011.
- [174] S. Azizi and E. Ahmadloo, “Prediction of heat transfer coefficient during condensation of R134a in inclined tubes using artificial neural network,” *Applied Thermal Engineering*, vol. 106, pp. 203–210, 2016.
- [175] E. Cho, H. Lee, M. Kang et al., “A neural network model for free-falling condensation heat transfer in the presence of non-condensable gases,” *International Journal of Thermal Sciences*, vol. 171, article 107202, 2022.
- [176] D. H. Lee, J. M. Yoo, H. Y. Kim, D. J. Hong, B. J. Yun, and J. J. Jeong, “Application of the machine learning technique for the development of a condensation heat transfer model for a passive containment cooling system,” *Nuclear Engineering and Technology*, vol. 54, no. 6, pp. 2297–2310, 2022.
- [177] S. A. Albdour, Y. Addad, S. Rabbani, and I. Afgan, “Machine learning-driven approach for predicting the condensation heat transfer coefficient (HTC) in the presence of non-condensable gases,” *International Journal of Heat and Fluid Flow*, vol. 106, article 109330, 2024.
- [178] S. Zhao, Y. Zhang, Y. Zhang, W. Zhang, J. Yang, and S. Kitipornchai, “Genetic programming-assisted micromechanical models of graphene origami-enabled metal metamaterials,” *Acta Materialia*, vol. 228, article 117791, 2022.
- [179] T. M. Alam, J. P. Allers, C. J. Leverant, and J. A. Harvey, “Symbolic regression development of empirical equations for diffusion in Lennard-Jones fluids,” *The Journal of Chemical Physics*, vol. 157, no. 1, article 014503, 2022.
- [180] A. D. Mehr, V. Nourani, E. Kahya, B. Hrnjica, A. M. Sattar, and Z. M. Yaseen, “Genetic programming in water resources engineering: a state-of-the-art review,” *Journal of Hydrology*, vol. 566, pp. 643–667, 2018.
- [181] J. Tang, S. Yu, and H. Liu, “Development of correlations for steam condensation over a vertical tube in the presence of noncondensable gas using machine learning approach,” *International Journal of Heat and Mass Transfer*, vol. 201, article 123609, 2023.